Surface wrinkling of a hyperelastic half-space coated by a liquid crystal elastomer film

Yang Liu[a,b], Qianqian Ji[a], Alain Goriely[b,*]

[a] *Department of Mechanics, School of Mechanical Engineering, Tianjin University, Tianjin 300354, China*
[b] *Mathematical Institute, University of Oxford, Oxford, OX2 6GG, UK*

Abstract

We consider the stability of a hyperelastic substrate coated by a liquid crystal elastomer film and subjected to compressive forces. In this problem, the liquid crystal elastomer directors are free to evolve and this possible variation needs to be included in the stability analysis. We consider the case where the initial directors are aligned either in the horizontal or in the vertical direction and obtain an exact bifurcation condition for surface wrinkling. We show that director reorientation increases both the critical compressive strain and the critical wavenumber, hence stabilizing the material. In the small wavenumber limit we carry out an asymptotic analysis and obtain analytical solutions for the critical stretch and the critical wavenumber, which can be useful in applications.

Keywords: surface instability, liquid crystal elastomer, incremental theory, finite elasticity, asymptotic analysis

1. Introduction

Liquid crystal elastomers (LCEs) combine the elasticity of rubber-like materials with the control features of liquid crystals (Warner and Terentjev, 2007). Depending on the arrangement of liquid crystal molecules, LCEs are classified as being in a nematic phase, smectic phase, or cholesteric phase. The nematic phase is the simplest since the director can be encoded by a single unit vector $\mathbf{n}$. Due to their fast and controllable reactions in response to various stimuli, such as mechanical loads (Conti et al., 2002; Ware et al., 2016), light (Sonnet and Virga, 2022; Liu et al., 2022), magnetic and electric fields (Urayama et al., 2005, 2006; Xu et al., 2020; Liu et al., 2020), and heating (Agrawal et al., 2014; Wang et al., 2017), LCEs have been suggested as promising materials in many applications such as artificial muscles (De Gennes et al., 1997; Tian et al., 2018), soft robotics (Zeng et al., 2018; DeSimone et al., 2015; Zhao et al., 2022), soft brakes (Wang et al., 2019; Pang et al., 2019), and 4D printing (Wang et al., 2022; chen et al., 2023). An excellent starting point for the interested reader is the monograph by Warner and Terentjev (2007).

Many interesting features of LCEs were unraveled through experiments (see White and Broer (2015) and Xiao et al. (2023) for background). Mitchell et al. (1993) observed that the director of an LCE sample rotates in the loading direction. Kundler and Finkelmann (1995) discovered the "striping phenomenon" in a uniaxial stretching experiment of LCEs which Fried and Sellers (2006) showed to be fundamental and independent of the material softness. Under light or temperature stimuli, bending, curling and rolling of LCE specimens can be induced (Potekhin and Wang, 2021;

*Corresponding author.
Email address: goriely@maths.ox.ac.uk (Alain Goriely)

Zhai et al., 2021). Further, an indentation on flat LCE samples will create an elastic bulging (Mihai et al., 2023).

In order to describe theoretically the deformation behaviour of LCEs, a constitutive model is needed (Ball and Bedford, 2015). Accordingly, various strain-energy functions for LCEs have been suggested. Warner et al. (1988) extended the classical Gaussian theory of rubber elasticity to obtain the *neo-classical strain-energy function* that describes the deformation of LCEs under mechanical loads. Anderson et al. (1999) developed a continuum theory of LCEs where the strain-energy function is dependent on the deformation gradient, the director, and the gradient of director. Zhang et al. (2019) proposed a general theory applicable to the dynamics of LCEs with large deformations, director rotations and an order parameter that depends on temperature and light. Mihai et al. (2022) extended the classical Ogden model for rubber to study the auxetic responses of stretch deformation of LCEs. Recently, Wang et al. (2022) developed a constitutive model to characterize viscoelastic behaviors of LCEs. Wu et al. (2023) presented a model to include the effect of loading-history dependence. Lee et al. (2023) proposed a macroscopic constitutive relation for polydomain LCEs. Since LCE samples are usually thin, there are many instances where they can be adequately modelled as plates. Indeed, the LCE samples made by Yan et al. (2012); Wang et al. (2017, 2019); Qing et al. (2019) are a few hundred micrometres in thickness. For this geometry, Krieger and Dias (2019) derived a von Kármán-type plate theory for LCEs and Mihai and Goriely (2020) developed a new plate theory by decomposing the deformation gradient into elastic and natural deformations, which allows for the consideration of both optical and mechanical loads. Liu et al (2020) proposed a consistent plate model for LCEs subjected to mechanical loads suitable for finite deformations and without specific restriction on the applied load. Finally, Goriely et al. (2023) derived a LCE rod model suitable to model illumination-induced deformations.

In general, the existence of directors and their deformations poses great challenges in solving the boundary value problems for such system. A way to bypass this problem is to carry out numerical simulations by modeling LCEs as a thermally sensitive material with anisotropic thermal expansions. Therefore, many commercial softwares can be directly used to study the mechanical behaviour of LCEs (Mbanga et al., 2010; Zhao et al., 2023; Peng et al., 2023). More recently, the effect of director was also included in such codes Chen et al. (2022). Further, Mahardika et al. (2024) performed a molecular dynamics simulation of deformations of LCEs under temperature effect.

As LCEs are typically thin, it is usual to support an LCE film by an elastic substrate, which creates a film-substrate bilayer. The surface wrinkling of bilayers has been of great interest in the last decades as it represents a fundamental instability in soft matter mechanics with a myriad of applications (Li et al., 2012; Goriely, 2017). An effective way to investigate such instabilities is to use the theory of incremental deformations, referred to as the small-on-large theory or incremental theory (Biot, 1965; Ogden, 1984). Within the framework of finite elasticity, Cai and Fu (1999) obtained a critical condition for the onset of surface wrinkling as well as the evolution of post-buckling of film/substrate structures. Since then, the effect of curvature (Jia et al., 2018), pre-stretch (Cao and Hutchinson, 2012), growth (Budday et al., 2015; Alawiye et al., 2019; Jin et al., 2019; Liu et al., 2021), fibers (Stewart et al., 2016) were studied using theoretical, numerical, and experimental techniques. For LCE structures, Agrawal et al. (2012) prepared a bilayer system where a thin polystyrene film attached to an LCE substrate and observed its wrinkling under temperature change using optical microscopy while Soni et al (2016) studied theoretically surface wrinkling in an elastic film bonded to an LCE substrate. Fu et al (2018) explored the surface instability of LCE thin film substrate systems under light loading and applied Fourier spectral methods to investigate the post-buckling evolution. Krieger and Dias (2019) investigated surface wrinkling of a substrate

coated by an LCE film using a plate model. Zhao et al. (2019) carried a finite element simulation for controllable surface patterns on LCE film-substrate structures by laser illumination. Xu and Zhao (2020) performed a finite element simulation on thermal wrinkling of LCE shell/core systems and studied the influence of director alignment on pattern selection. Starting from finite elasticity, Goriely and Mihai (2021) carried out a bifurcation analysis of a bilayer under biaxial compression where either the film or the substrate can be composed of LCEs. In particular, asymptotic solutions of the critical stretch triggering surface wrinkling as well as the critical wavenumber were deduced. In this model the director is assumed to be anchored. Barnes et al. (2023) conducted a systematic exploration on surface instabilities of LCE film-substrate structure generated in heating or cooling processes, and both experiments and numerical simulations were performed. In general, rotations of the director are possible which motivates the current study.

Here, we consider the coupling effect of director rotation of LCEs and the mechanical deformation induced by external loads. We develop a general incremental theory for LCEs within the framework of finite elasticity. Then, we conduct a standard bifurcation analysis to study the influence of various parameters on the onset and pattern obtained during wrinkling.

2. Problem formulation

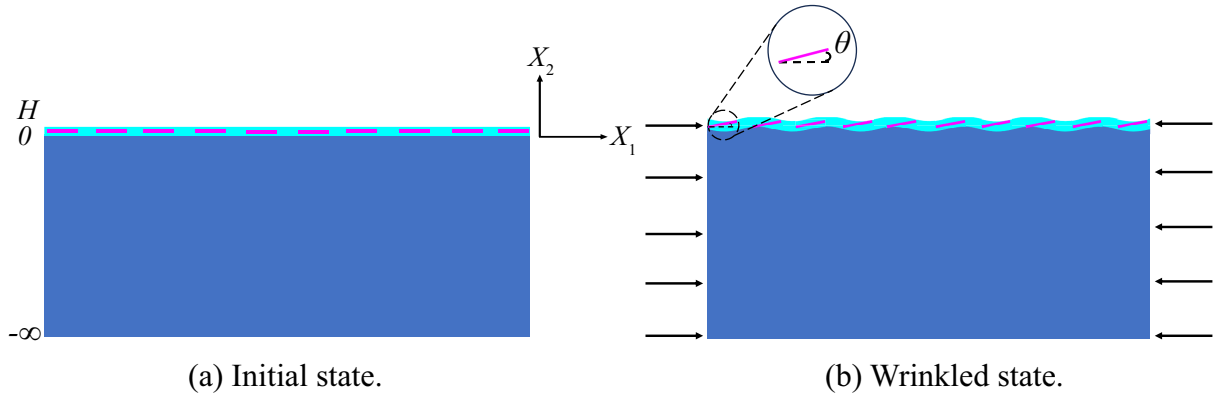

Figure 1: Illustration of an LCE-substrate structure. (a) Initial state, where no force is applied to the structure; (b) Wrinkled state, where surface wrinkling is created by applied axial compression.

We consider an LCE film bonded to a hyperelastic incompressible half-space. The thickness of the film in the initial configuration B_0 is denoted by H. We assume that the bilayer undergoes a plane-strain deformation generated by a uniform compression, and as a result the thickness of the film becomes h in the current configuration B_1. As the compressive stress reaches a critical value, an instability takes place resulting in surface wrinkling (see Figure 1).

We model the LCE film as an incompressible materials with a director field (Warner et al., 1988; Bladon et al., 1993; Anderson et al., 1999). Therefore, our problem is the generalisation of the classical elastic incompressible bilayer problem under compression to the case where the film also includes directors. To distinguish between the LCE film and the substrate, we refer to any quantities related to the substrate by a hat " ˆ ", and without a hat for the LCE film. For example, the strain-energy function of the LCE layer is written as W and the counterpart of the substrate is represented by $\hat{W}$.

For our problem, it is convenient to use a Cartesian coordinate system in both the reference and the current configurations. Accordingly, the position vectors of a material point in B_0 and B_1

are denoted by $\mathbf{X} = (X_1, X_2)$ and $\mathbf{x} = (x_1, x_2)$, respectively. The same orthonormal basis $\{\mathbf{E}_1, \mathbf{E}_2\}$ in all configurations will be used.

For the LCE film, we adopt the neo-classical constitutive model proposed by Warner et al. (1988) with an equivalent strain-energy function for isothermal deformation (Bladon et al., 1993; Fried and Korchagin, 2002):

$$W = \frac{\mu}{2}\left(\mathrm{tr}\left(\mathbf{F}\mathbf{F}^{\mathrm{T}}\right) - \frac{s-1}{s}\mathbf{F}^{\mathrm{T}}\mathbf{n}\cdot\mathbf{F}^{\mathrm{T}}\mathbf{n} + (s-1)\mathbf{F}\mathbf{n}_0\cdot\mathbf{F}\mathbf{n}_0 - \frac{(s-1)^2}{s}\left(\mathbf{F}^{\mathrm{T}}\mathbf{n}\cdot\mathbf{n}_0\right)^2 - 3\right), \quad (2.1)$$

where μ denotes the ground-state shear modulus, $\mathbf{F}$ is the deformation gradient, $\mathbf{n}_0$ and $\mathbf{n}$ are the directors in the reference and the deformed configurations, respectively, s is a positive parameter measuring anisotropy, and the superscript 'T' stands for transpose. When $s = 1$, (2.1) reduces to energy density of the neo-Hookean model. The liquid crystal molecules are oblate if $s < 1$ and prolate if $s > 1$. We further assume that the directors $\mathbf{n}_0$ and $\mathbf{n}$ are both unit vectors that are in the (X_1, X_2)-plane.

For the substrate, we use the incompressible neo-Hookean model:

$$\hat{W} = \frac{\hat{\mu}}{2}\left(\mathrm{tr}\left(\hat{\mathbf{F}}\hat{\mathbf{F}}^{\mathrm{T}}\right) - 3\right), \quad (2.2)$$

where $\hat{\mu}$ represents the ground-state shear modulus of the substrate.

The nominal stress tensors of the LCE film and of the substrate are given by

$$\mathbf{S} = \frac{\partial W(\mathbf{F}, \mathbf{n})}{\partial \mathbf{F}} - p\mathbf{F}^{-1}, \quad \hat{\mathbf{S}} = \frac{\partial \hat{W}(\hat{\mathbf{F}})}{\partial \hat{\mathbf{F}}} - \hat{p}\hat{\mathbf{F}}^{-1}, \quad (2.3)$$

where the pressures p and $\hat{p}$ arise from the incompressibility constraints $\det \mathbf{F} = 1$ and $\det \hat{\mathbf{F}} = 1$. An important difference with a typical elastic theory is the appearance of internal orientational body-force density for the LCE film given by

$$\mathbf{\Pi} = -\frac{\partial W(\mathbf{F}, \mathbf{n})}{\partial \mathbf{n}} - p_1\mathbf{n}, \quad (2.4)$$

where p_1 is the Lagrange multiplier enforcing the constraint $\mathbf{n}\cdot\mathbf{n} = 1$.

2.1. Homogeneous deformation

We first study the homogeneous deformation and characterize the current finite-deformation state B_1. All physical quantities associated with B_1 will be added on an overbar "$-$". In view of the fact that both layers are incompressible, i.e. $\det \bar{\mathbf{F}} = 1$, the deformation gradient valid for both the LCE film and the half-space reads

$$\bar{\mathbf{F}} = \begin{pmatrix} \lambda & 0 \\ 0 & 1/\lambda \end{pmatrix}, \quad (2.5)$$

where λ is a constant principal stretch in the X_1-direction. The counterpart in the X_2-direction is then $1/\lambda$. We immediately find that the deformed thickness $h = H/\lambda$. Whenever a quantity in the substrate and in the film take the same value, we will discard the upper hat to denote both.

For the director, we have

$$\mathbf{n}_0 = \cos\theta_0\mathbf{E}_1 + \sin\theta_0\mathbf{E}_2, \quad \bar{\mathbf{n}} = \cos\bar{\theta}\mathbf{E}_1 + \sin\bar{\theta}\mathbf{E}_2, \quad (2.6)$$

where θ_0 and $\bar{\theta}$ denote the angles between the director and the horizontal direction $\mathbf{E}_1$ in the initial configuration B_0 and the reference configuration B_1, respectively.

The nominal stresses $\bar{\mathbf{S}}$ and $\hat{\bar{\mathbf{S}}}$ are also constant tensors. Hence for a static problem, the two equilibrium equations

$$\operatorname{Div}\bar{\mathbf{S}}=\mathbf{0},\quad \operatorname{Div}\hat{\bar{\mathbf{S}}}=\mathbf{0} \tag{2.7}$$

are trivially satisfied. Note that "Div" is the divergence operator with respect to the coordinates in B_0. We further study the orientational momentum balance which results in the equation $\bar{\mathbf{\Pi}}=\mathbf{0}$ for the material constitutive model (2.1) (Anderson et al., 1999). Further, we emphasize that the multiplier arising from the constraint of the director is negligible as shown in Anderson et al. (1999); Chen and Fried (2006). To eliminate p_1 in (2.4), we apply a projection operator $(\mathbf{I}-\bar{\mathbf{n}}\otimes\bar{\mathbf{n}})$ on $\bar{\mathbf{\Pi}}=\mathbf{0}$ to find (Liu et al, 2020)

$$(\mathbf{I}-\bar{\mathbf{n}}\otimes\bar{\mathbf{n}})\frac{\partial W(\bar{\mathbf{F}},\bar{\mathbf{n}})}{\partial\bar{\mathbf{n}}}=\mathbf{0}. \tag{2.8}$$

In the light of (2.1), (2.5), and (2.6), equation (2.8) gives rise to the following scalar equation

$$(s-1)\cos 2\bar{\theta}\sin 2\theta_0-\frac{\sin 2\bar{\theta}\Big(\left(\lambda^4+1\right)(s-1)\cos 2\theta_0+\left(\lambda^4-1\right)(s+1)\Big)}{2\lambda^2}=0. \tag{2.9}$$

We then immediately obtain

$$\tan 2\bar{\theta}=\frac{2(s-1)\lambda^2\sin 2\theta_0}{(1+s)\left(\lambda^4-1\right)+(s-1)\left(\lambda^4+1\right)\cos 2\theta_0}. \tag{2.10}$$

It can be seen from (2.10) that if $\theta_0=0$ or $\theta_0=\pi/2$ the only possible solution is $\bar{\theta}=0$ or $\bar{\theta}=\pi/2$ (as we are only concerned with $0\leqslant\bar{\theta}\leqslant\pi/2$). It implies that a director reorientation may be triggered whenever the initial director is either parallel or perpendicular to the X_1-axis. We emphasize that such phenomenon was also discovered in compressed bilayers (Mihai and Goriely, 2021; Goriely and Mihai, 2021), in inflated LCE tubes (Chen and Fried, 2006), and in the bending of LCEs (Liu et al, 2021). We refer to Mihai and Goriely (2021) for a detailed discussion on the parameter selections needed to avoid director reorientation.

In the following analysis, we focus on the special case where the initial angle is $\theta_0=0$ ($\mathbf{n}_0=\mathbf{E}_1$) or $\theta_0=\pi/2$ ($\mathbf{n}_0=\mathbf{E}_2$). Consequently, there are four homogeneous solutions characterized by: $\{\theta_0=0,\bar{\theta}=0\}$, $\{\theta_0=0,\bar{\theta}=\pi/2\}$, $\{\theta_0=\pi/2,\bar{\theta}=0\}$, and $\{\theta_0=\pi/2,\bar{\theta}=\pi/2\}$.

For these solutions, Equation $(2.3)_1$ yields

$$\begin{aligned}
\bar{\mathbf{S}}&=\begin{pmatrix}\lambda\mu-\dfrac{\bar{p}}{\lambda} & 0\\ 0 & \dfrac{\mu}{\lambda}-\lambda\bar{p}\end{pmatrix},\quad \text{for}\ \ \{\theta_0=0,\ \bar{\theta}=0\}\ \text{or}\ \{\theta_0=\pi/2,\ \bar{\theta}=\pi/2\},\\
\bar{\mathbf{S}}&=\begin{pmatrix}s\lambda\mu-\dfrac{\bar{p}}{\lambda} & 0\\ 0 & \dfrac{\mu}{s\lambda}-\lambda\bar{p}\end{pmatrix},\quad \text{for}\ \ \{\theta_0=0,\ \bar{\theta}=\pi/2\},\\
\bar{\mathbf{S}}&=\begin{pmatrix}\dfrac{\lambda\mu}{s}-\dfrac{\bar{p}}{\lambda} & 0\\ 0 & \dfrac{s\mu}{\lambda}-\lambda\bar{p}\end{pmatrix},\quad \text{for}\ \ \{\theta_0=\pi/2,\ \bar{\theta}=0\}.
\end{aligned} \tag{2.11}$$

Accordingly, the nominal stress for the substrate is

$$\hat{\bar{\mathbf{S}}} = \begin{pmatrix} \lambda\hat{\mu} - \hat{\bar{p}}/\lambda & 0 \\ 0 & \hat{\mu}/\lambda - \lambda\hat{\bar{p}} \end{pmatrix}. \tag{2.12}$$

Next, we consider the boundary and interface conditions. We assume that the upper surface is traction-free and the interface remains bonded which implies that continuity conditions are imposed at the interface. For the homogeneous deformation, we have

$$\bar{S}_{22}\big|_{X_2=H} = 0, \quad \left(\bar{S}_{22} - \hat{\bar{S}}_{22}\right)\big|_{X_2=0} = 0, \tag{2.13}$$

from which we obtain

$$\begin{aligned} &\hat{\bar{p}} = \frac{\hat{\mu}}{\lambda^2}, \quad \bar{p} = \frac{\mu}{\lambda^2}\ (\{\theta_0 = 0,\ \bar{\theta} = 0\} \text{ or } \{\theta_0 = \pi/2,\ \bar{\theta} = \pi/2\}), \\ &\bar{p} = \frac{\mu}{s\lambda^2},\ (\{\theta_0 = 0,\ \bar{\theta} = \pi/2\}), \quad \bar{p} = \frac{s\mu}{\lambda^2},\ (\{\theta_0 = \pi/2,\ \bar{\theta} = 0\}). \end{aligned} \tag{2.14}$$

As there are two solutions $\bar{\theta} = 0$ and $\bar{\theta} = \pi/2$, it is necessary to identify which one is the favorable one by computing the total energy of each solution. We select a representative block area from the original structure with $[-L, L] \times [0, H] \cup [-L, L] \times [-50H, 0]$. The equivalence to the prototypical problem can be attained by applying periodic conditions at the two lateral sides. For a displacement-control problem, the dimensionless two-dimensional energy is

$$\Psi = \frac{\Psi^*}{LH\hat{\mu}} = \Psi_1 + \Psi_2 = \frac{1}{LH\hat{\mu}}\left(\int_{-L}^{L}\int_{0}^{H} W \mathrm{d}X_1\mathrm{d}X_2 + \int_{-L}^{L}\int_{-50H}^{0} \hat{W}\mathrm{d}X_1\mathrm{d}X_2\right). \tag{2.15}$$

When the director $\mathbf{n}_0$ is initially aligned in $\mathbf{E}_1$-direction, with the use of (2.1) and (2.2), the corresponding energy for the two solutions $\bar{\theta} = 0$ and $\bar{\theta} = \pi/2$ read

$$\Psi_0^0 = \frac{(\beta + 50)\left(\lambda^2 - 1\right)^2}{\lambda^2}, \quad \Psi_{\pi/2}^0 = \frac{50\left(\lambda^2 - 1\right)^2}{\lambda^2} + \beta\left(\lambda^2 s + \frac{1}{\lambda^2 s} - 2\right), \tag{2.16}$$

where the superscript and subscript correspond to the initial and deformed directors, respectively, and $\beta = \mu/\hat{\mu}$ is the modulus ratio between two layers, an important parameter in the wrinkling problem.

It follows from (2.16) that Ψ_0^0 is lower than $\Psi_{\pi/2}^0$ as $\lambda > s^{-1/4}$, and the only positive real solution to $\Psi_0^0 = \Psi_{\pi/2}^0$ is $\lambda = s^{-1/4}$. Therefore, we conclude that a director reorientation (director jumps from $\mathbf{E}_1$ to $\mathbf{E}_2$) is possible only if $s > 1$. Furthermore, if the director $\mathbf{n}_0$ is initially aligned in the $\mathbf{E}_2$-direction, we find that

$$\Psi_0^{\pi/2} = \frac{50\left(\lambda^2 - 1\right)^2}{\lambda^2} + \beta\left(\frac{\lambda^2}{s} + \frac{s}{\lambda^2} - 2\right), \quad \Psi_{\pi/2}^{\pi/2} = \frac{(\beta + 50)\left(\lambda^2 - 1\right)^2}{\lambda^2}. \tag{2.17}$$

In this scenario ($\mathbf{n}_0 = \mathbf{E}_2$), we find that a director reorientation (with a jump from $\mathbf{E}_2$ to $\mathbf{E}_1$) can only be initiated if $s < 1$ and the critical compressive stretch is $\lambda = s^{1/4}$.

2.2. Incremental theory

The incremental theory for hyperelastic material is now well established and we refer the reader to the excellent description found in (Ogden, 1984; Fu and Ogden, 1999). Therefore, we shall not repeat all the steps here but, instead, we will follow the standard procedure to obtain the required equations and boundary conditions. Here we need to extend the fundamental theory to the case of LCE film for which we have the added complication introduced by the director field. Therefore, we will only include this novel aspect for the film while the counterpart for the substrate will be given without derivation.

We expect that a wrinkling instability will be triggered as the applied deformation increases. To characterize the onset of instability, we superimpose an incremental displacement $\mathbf{u} = [u_1, u_2]^{\mathrm{T}}$ and an incremental director by $\mathbf{m} = [m_1, m_2]^{\mathrm{T}}$ on B_1.The resulting configuration is called B_2. The position vector for a representative material particle in B_2 is represented by $\widetilde{\mathbf{x}}$ and the associated director by $\mathbf{n}$. We have

$$\mathbf{u}(x_1, x_2) = \widetilde{\mathbf{x}}(x_1, x_2) - \mathbf{x}, \quad \mathbf{m}(x_1, x_2) = \mathbf{n}(x_1, x_2) - \bar{\mathbf{n}}. \tag{2.18}$$

It then follows that the deformation gradient $\mathbf{F}$ arising from $B_0 \longrightarrow B_2$ is

$$\mathbf{F} = (\mathbf{I} + \boldsymbol{\eta})\bar{\mathbf{F}}, \tag{2.19}$$

where $\mathbf{I}$ is the second-order identity tensor and $\boldsymbol{\eta}$ the displacement gradient tensor with components $\eta_{ij} = u_{i,j}$. Here, the comma denotes derivative with respect to the implied coordinates. Based on $(2.18)_2$, the internal orientational body-force density in B_2 (2.4) can be replaced by

$$\boldsymbol{\Pi} = -\frac{\partial W(\mathbf{F}, \mathbf{n})}{\partial \mathbf{n}} - p_1(\mathbf{m} + \bar{\mathbf{n}}). \tag{2.20}$$

To obtain the incremental equations applicable to the LCE film, we first define the incremental nominal stress

$$\dot{\mathbf{S}} = \bar{J}^{-1}\bar{\mathbf{F}}(\mathbf{S} - \bar{\mathbf{S}}), \tag{2.21}$$

where $\bar{J} = \det \bar{\mathbf{F}}$, which is one in this problem but is still kept so that the formula can be easily generalized. Similarly, we define the internal orientational body-force density increment by

$$\dot{\boldsymbol{\Pi}} = \bar{J}^{-1}(\boldsymbol{\Pi} - \bar{\boldsymbol{\Pi}}) = \bar{J}^{-1}\left(-\frac{\partial W}{\partial \mathbf{n}} + \frac{\partial W}{\partial \bar{\mathbf{n}}} - p_1^*\bar{\mathbf{n}} - p_1\mathbf{m}\right). \tag{2.22}$$

Note that we have used $p_1^* = p_1 - \bar{p}_1$ in the above equation.

To eliminate the Lagrange multipliers generated by the constraint of director, we use the constraint $\mathbf{n} \cdot \mathbf{n} = 1$ which gives

$$\mathbf{m} \cdot (2\bar{\mathbf{n}} + \mathbf{m}) = 0. \tag{2.23}$$

Next, applying the two tensors $\mathbf{I} - \mathbf{a} \otimes \mathbf{a}/(\mathbf{a} \cdot \mathbf{a})$ and $\mathbf{I} - \mathbf{m} \otimes \mathbf{m}/(\mathbf{m} \cdot \mathbf{m})$ with $\mathbf{a} = \bar{\mathbf{n}} + \mathbf{m}/2$ (Liu et al, 2020) and using (2.23) we obtain the incremental equations:

$$\begin{aligned} &\operatorname{div} \dot{\mathbf{S}} = \mathbf{0}, \\ &\left(\mathbf{I} - \mathbf{a} \otimes \frac{\mathbf{a}}{\mathbf{a} \cdot \mathbf{a}}\right)\left(\mathbf{I} - \mathbf{m} \otimes \frac{\mathbf{m}}{\mathbf{m} \cdot \mathbf{m}}\right)\dot{\widetilde{\boldsymbol{\Pi}}} = \mathbf{0}, \quad \text{with} \quad \dot{\widetilde{\boldsymbol{\Pi}}} \equiv -\frac{\partial W}{\partial \mathbf{n}} + \frac{\partial W}{\partial \bar{\mathbf{n}}}, \end{aligned} \tag{2.24}$$

where "div" denotes the divergence operator with respect to the coordinates in B_1.

We denote by p^* the incremental pressure for the LCE film such that $p = \bar{p} + p^*$ in B_2 and taking the series expansions of $\dot{\mathbf{S}}$ and $\widetilde{\dot{\mathbf{\Pi}}}$ in terms of $(\bar{\mathbf{F}}, \bar{\mathbf{n}})$ to first order, we obtain (Ogden, 1984; Fu and Ogden, 1999):

$$\begin{aligned}
&\dot{S}_{ji} = \mathscr{A}_{jilk} u_{k,l} + \bar{p} u_{j,i} - p^* \delta_{ji} + \mathscr{B}_{jik} m_k, \\
&\widetilde{\dot{\Pi}}_k = -\mathscr{B}_{ljk} u_{j,l} - \mathscr{C}_{kj} m_j,
\end{aligned} \tag{2.25}$$

where δ_{ji} is the Kronecker delta, and $\mathscr{A}_{jilk}$, $\mathscr{B}_{jik}$, $\mathscr{C}_{ji}$ are the first-order instantaneous elastic moduli defined by

$$\mathscr{A}_{jilk} = \bar{J}^{-1} \bar{F}_{jA} \bar{F}_{lB} \frac{\partial^2 W}{\partial F_{iA} \partial F_{kB}}\bigg|_{\mathbf{F}=\bar{\mathbf{F}}, \mathbf{n}=\bar{\mathbf{n}}}, \ \mathscr{B}_{jik} = \bar{J}^{-1} \bar{F}_{jA} \frac{\partial^2 W}{\partial F_{iA} \partial n_k}\bigg|_{\mathbf{F}=\bar{\mathbf{F}}, \mathbf{n}=\bar{\mathbf{n}}}, \ \mathscr{C}_{ji} = \bar{J}^{-1} \frac{\partial^2 W}{\partial n_j \partial n_i}\bigg|_{\mathbf{F}=\bar{\mathbf{F}}, \mathbf{n}=\bar{\mathbf{n}}}. \tag{2.26}$$

Accordingly, the incremental equations (2.24) transform into

$$\begin{aligned}
&\mathscr{A}_{jilk} u_{k,lj} - p^*_i + \mathscr{B}_{jik} m_{k,j} = 0, \\
&(\delta_{ik} - \bar{n}_i \otimes \bar{n}_k)(-\mathscr{B}_{ljk} u_{j,l} - \mathscr{C}_{kl} m_l) = 0.
\end{aligned} \tag{2.27}$$

The linearized incompressibility condition and the unit director constraint are prescribed by

$$u_{i,i} = 0, \quad m_i \cdot \bar{n}_i = 0. \tag{2.28}$$

The incremental boundary conditions at the upper surface and continuity conditions at the interface lead to

$$\mathbf{T}\big|_{x_2=h} = \mathbf{0}, \quad (\mathbf{T} - \hat{\mathbf{T}})\big|_{x_2=0} = \mathbf{0}, \quad (\mathbf{u} - \hat{\mathbf{u}})\big|_{x_2=0} = 0, \tag{2.29}$$

where $\mathbf{T} = \dot{\mathbf{S}}^{\mathrm{T}} \mathbf{E}_2$ is the traction vector and $\hat{\mathbf{T}}$ the counterpart for the substrate with components given by

$$\begin{aligned}
T_i =& \mathscr{A}_{2ilk} u_{k,l} + \bar{p} u_{2,i} - p^* \delta_{2i} + \mathscr{B}_{2ik} m_k, \\
\hat{T}_i =& \hat{\mathscr{A}}_{2ilk} \hat{u}_{k,l} + \hat{\bar{p}} \hat{u}_{2,i} - \hat{p}^* \delta_{2i}.
\end{aligned}$$

Finally, we write the incremental equations for the substrate and the associated decaying condition at infinity as

$$\begin{aligned}
&\hat{u}_{i,i} = 0, \quad \hat{\mathscr{A}}_{jilk} \hat{u}_{k,lj} - \hat{p}^*_{,i} = 0, \\
&\hat{u}_i \to 0, \quad \text{as } x_2 \to -\infty.
\end{aligned} \tag{2.30}$$

3. Bifurcation analysis

We are now in a position to carry out a bifurcation analysis based on the incremental governing system (2.27)-(2.30). We will take $\theta_0 = 0$ as an example. In this case, there is no director reorientation, $\bar{\theta} = 0$, and $(2.28)_2$ gives rise to $m_1 = 0$. As a result, we look for a solution of the form

$$\begin{aligned}
&u_1 = \mathrm{e}^{\mathrm{i}kx_1} k U'(kx_2), \quad u_2 = -\mathrm{i}k\mathrm{e}^{\mathrm{i}kx_1} U(kx_2), \\
&\hat{u}_1 = \mathrm{e}^{\mathrm{i}kx_1} k \hat{U}'(kx_2), \quad \hat{u}_2 = -\mathrm{i}k\mathrm{e}^{\mathrm{i}kx_1} \hat{U}(kx_2), \\
&m_2 = \mathrm{e}^{\mathrm{i}kx_1} V(x_2),
\end{aligned} \tag{3.1}$$

where 'i' is the imaginary unit, primes denote derivative with respect to the implied variable, k stands for the wavenumber, U, $\hat{U}$ and V are unknown functions. A direct computation would show that the incompressibility condition is automatically satisfied by (3.1).

Substituting (3.1) into (2.27), $(2.30)_2$ and eliminating p^*, $\hat{p}^*$ through cross differentiation result in

$$\begin{aligned}
&k^4 s^2 \lambda^4 U - k^2(s-1)s\lambda^4 V - k^4 s(\lambda^4+1)U'' + k^2(1-s)V'' + k^4 U'''' = 0,\\
&(s-1)(k^2 s\lambda^4 U + V + k^2 U'') = 0,\\
&\lambda^4 \hat{U} - \left(\lambda^4+1\right)\hat{U}'' + \hat{U}'''' = 0.
\end{aligned} \tag{3.2}$$

We eliminate V in $(3.2)_1$ by using $(3.2)_2$. As a result, the general solutions of U and $\hat{U}$ can be formulated by solving the associated eigenvalue problems of $(3.2)_1$ and $(3.2)_3$:

$$\begin{aligned}
U(kx_2) &= C_1 \mathrm{e}^{-\gamma_1 k x_2} + C_2 \mathrm{e}^{\gamma_1 k x_2} + C_3 \mathrm{e}^{-\gamma_2 k x_2} + C_4 \mathrm{e}^{\gamma_2 k x_2},\\
\hat{U}(kx_2) &= C_5 \mathrm{e}^{k x_2} + C_6 \mathrm{e}^{\lambda^2 k x_2} + C_7 \mathrm{e}^{-k x_2} + C_8 \mathrm{e}^{-k\lambda^2 x_2},
\end{aligned} \tag{3.3}$$

where C_i $(i = 1, 2\cdots, 8)$ are constants and the eigenvalues γ_1 and γ_2 are given by

$$\gamma_1 = \left(\frac{1+(3-2s)\lambda^4 - \sqrt{1+(6-8s)\lambda^4+(9-8s)\lambda^8}}{2}\right)^{1/2},$$

$$\gamma_2 = \left(\frac{1+(3-2s)\lambda^4 + \sqrt{1+(6-8s)\lambda^4+(9-8s)\lambda^8}}{2}\right)^{1/2}.$$

The decaying condition $(2.30)_3$ leads to $C_7 = C_8 = 0$.

Subsequently, we substitute (3.3) into the boundary conditions and continuity conditions (2.29) to obtain an algebraic system of the general form

$$\mathbf{M}_1 \cdot \mathbf{C} = 0 \tag{3.4}$$

where $\mathbf{C} = [C_1, C_2, C_3, C_4, C_5, C_6]^{\mathrm{T}}$ and the coefficient matrix $\mathbf{M}_1$ is given in (A.1). In order to find a non-trivial solution of the incremental displacements, the determinant of this matrix must vanish, resulting in the following bifurcation condition:

$$\det \mathbf{M}_1 \equiv f_1(\lambda, kh, \beta, s) = 0. \tag{3.5}$$

Since the bifurcation condition depends on k and h only via kh, we henceforth take kh as a single parameter.

From the previous section, we know that for some values of $s > 1$, the director will rotate from 0 to $\pi/2$ at $\lambda = s^{-1/4}$. If this value is more than the critical stretch triggering surface wrinkling, we may expect a director rotation first and then a secondary instability. For this special case, $(2.28)_2$ yields $m_2 = 0$ and therefore we shall seek a new increment $m_1 = \mathrm{e}^{\mathrm{i}kx_1} V(x_2)$. Accordingly, the general solution of the LCE film is replaced by

$$U(kx_2) = C_1 \mathrm{e}^{-\gamma_3 k x_2} + C_2 \mathrm{e}^{\gamma_3 k x_2} + C_3 \mathrm{e}^{-\gamma_4 k x_2} + C_4 \mathrm{e}^{\gamma_4 k x_2}, \tag{3.6}$$

where γ_3 and γ_4 are eigenvalues defined by

$$\gamma_3 = \left(\frac{s^2\lambda^4 + 3 - 2s - \left(\lambda^8 s^4 - 8\lambda^4 s^3 + 6\lambda^4 s^2 - 8s + 9\right)^{1/2}}{2(s^2\lambda^4 + s - 1)}\right)^{1/2} \lambda^2 s^{1/2},$$

$$\gamma_4 = \left(\frac{s^2\lambda^4 + 3 - 2s + \left(\lambda^8 s^4 - 8\lambda^4 s^3 + 6\lambda^4 s^2 - 8s + 9\right)^{1/2}}{2(s^2\lambda^4 + s - 1)}\right)^{1/2} \lambda^2 s^{1/2}.$$

Analogously, the bifurcation condition where surface instability occurs can be obtained from (2.29):

$$\det \mathbf{M}_2 \equiv f_2(\lambda, kh, \beta, s) = 0, \tag{3.7}$$

where $\mathbf{M}_2$ is shown in (A.2).

For the case $\theta_0 = \pi/2$, there are also two possible situations, i.e. $\bar{\theta} = \pi/2$ and $\bar{\theta} = 0$. The associated bifurcation conditions can be deduced by the same procedures and hence the details will be omitted. We directly write them as

$$\det \mathbf{M}_3 \equiv f_3(\lambda, kh, \beta, s) = 0, \quad \bar{\theta} = \frac{\pi}{2}, \tag{3.8}$$

$$\det \mathbf{M}_4 \equiv f_4(\lambda, kh, \beta, s) = 0, \quad \bar{\theta} = 0, \tag{3.9}$$

where $\mathbf{M}_3$ and $\mathbf{M}_4$ can be found in (A.3) and (A.4), respectively.

Using the bifurcation conditions (3.5) and (3.7)-(3.9), we can graph the bifurcation curves with varying kh as shown in Figure 2. We see that a director reorientation takes place before surface wrinkling when $\theta_0 = 0, s = 2$ and $\theta_0 = \pi/2, s = 0.8$ in Figure 2(a) and when $\theta_0 = \pi/2, s = 0.8$ in Figure 2(b). In the first case ($\beta = 1$), the LCE film and the substrate have the same modulus. When $s = 1$, the problem further reduces to a homogeneous half-space for which surface wrinkling occurs at the classical Biot value $\lambda \approx 0.5437$ (Biot, 1963). Therefore, we refer to the critical stretch for surface instability when $\beta = 1$ as λ_{Biot}. It can be seen from Figure 2(a) that all bifurcation curves intersect when $kh \to 0$ and the corresponding stretch is exactly at the Biot value 0.5437 (marked by a black point). In addition, if $s < 1$ and $\theta_0 = 0$ the principal stretch λ will converge to a limiting value as $kh \to \infty$, which is higher than 0.5437. Besides, the limit values as $kh \to \infty$ are lower than 0.5437 for the rest of bifurcation curves, and hence the critical stretch is $\lambda_{\text{Biot}} = 0.5437$. Correspondingly, the associated critical wavenumber is zero. A zero wavenumber will typically cause a localized instability, such as ridge formation in a film bonded to a pre-compressed substrate (Fu et al., 2023) and localized necking/bulging in circular cylinders (Fu et al., 2021; Liu and Dorfmann, 2023). We further show λ_{Biot} as a function of s in Figure 3. The black curve is monotonically decreasing with s until the Biot value is reached at $s = 1$ while the red one is a horizontal line. Moreover, the black curve is always higher, indicating that the LCE-substrate bilayer is more stable when the director is initially along the $\mathbf{E}_2$-direction. Note that the director will reorientate if $\theta_0 = \pi/2$ and $s < 1$. This further demonstrates that director reorientation stabilizes the material.

When the LCE film is stiffer than the substrate, as shown in Figure 2(b) the $\lambda - kh$ curve has a local maximum. We refer to this point as $(\lambda_{\text{cr}}, (kh)_{\text{cr}})$ with critical stretch λ_{cr} and critical wavenumber $(kh)_{\text{cr}}$. Next, we shall focus on the effect of parameters on this critical pattern.

3.1. Critical wrinkled state if the initial director is aligned in the horizontal direction

We first specify $\theta_0 = 0$ and use equations (3.5) and (3.7) to study the critical pattern. The pair $\{\lambda_{\text{cr}}, (kh)_{\text{cr}}\}$ can be determined from

$$f_i(\lambda, kh, \beta, s) = 0, \quad \frac{\partial f_i(\lambda, kh, \beta, s)}{\partial (kh)} = 0, \quad i = 1, 2. \tag{3.10}$$

We can solve these equations numerically for the critical stretch λ_{cr} and the critical wavenumber $(kh)_{\text{cr}}$. From (2.16) we know that a director jump from $\bar{\theta} = 0$ to $\bar{\theta} = \pi/2$ may take place at $\lambda = s^{-1/4}$ when $s > 1$. Therefore, we study separately the cases $s < 1$ and $s > 1$.

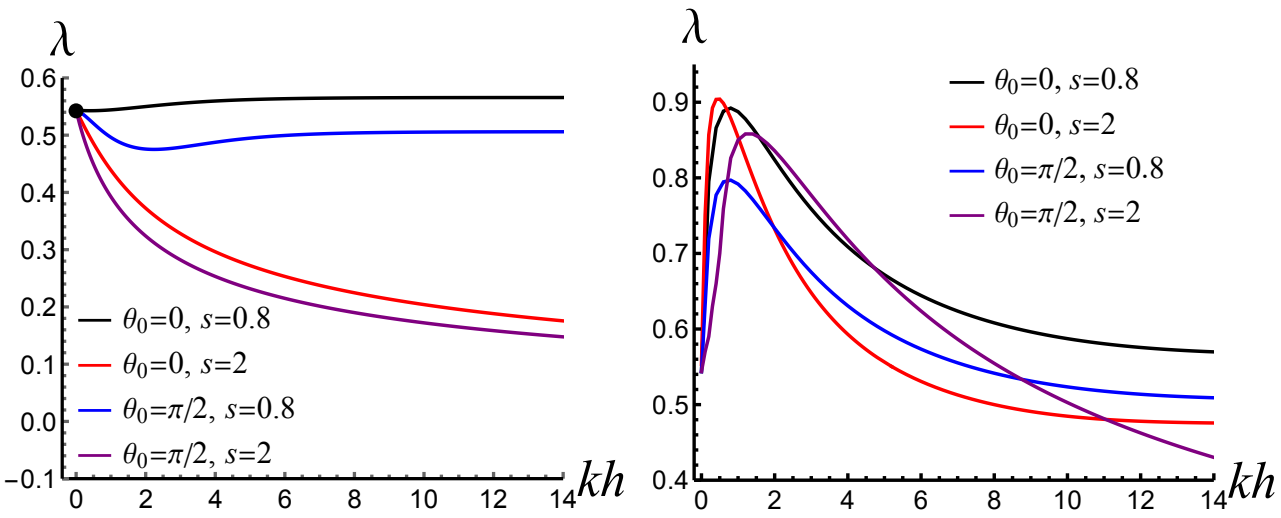

(a) $\beta = 1$. (b) $\beta = 10$.

Figure 2: Bifurcation curves for λ as a function of kh.

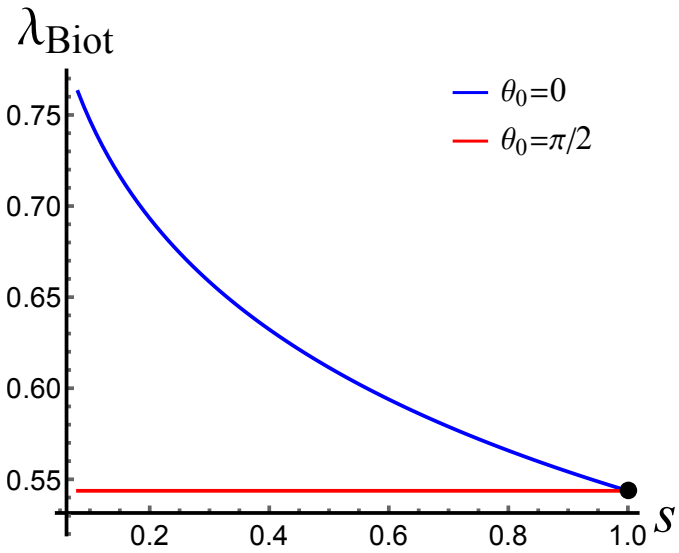

Figure 3: The Biot-like value curves for $\mathbf{n}_0 = \mathbf{E}_1$ (the black line) and $\mathbf{n}_0 = \mathbf{E}_2$ (the red line) when $s \leqslant 1$.

3.1.1. The case of $s < 1$

First, we assume $s < 1$ when the director remains in its initial direction before surface wrinkling. In that case, the critical stretch and the critical wavenumber are shown in Figure 4 based on equations (3.10) with $i = 1$. As can be appreciated from Figure 4(a), when the LCE film is stiffer than the substrate, the critical stretch $\lambda_{\rm cr}$ increases with β regardless of the value of s, implying that the bilayer becomes more unstable as the modulus ratio β increases. This is a well-known property of film-substrate structures (Cai and Fu, 1999; Andres et al., 2018; Wang et al., 2023) which remains valid when a substrate is coated by an LCE film (Krieger and Dias, 2019; Goriely and Mihai, 2021). Meanwhile, the value of s has a weak influence on $\lambda_{\rm cr}$ provided that β is large enough, which has also been observed by Goriely and Mihai (2021). As β decreases, the curve will intersect the horizontal line $\lambda = \lambda_{\rm Biot}$ and as a result the critical stretch will be replaced by $\lambda_{\rm Biot}$.

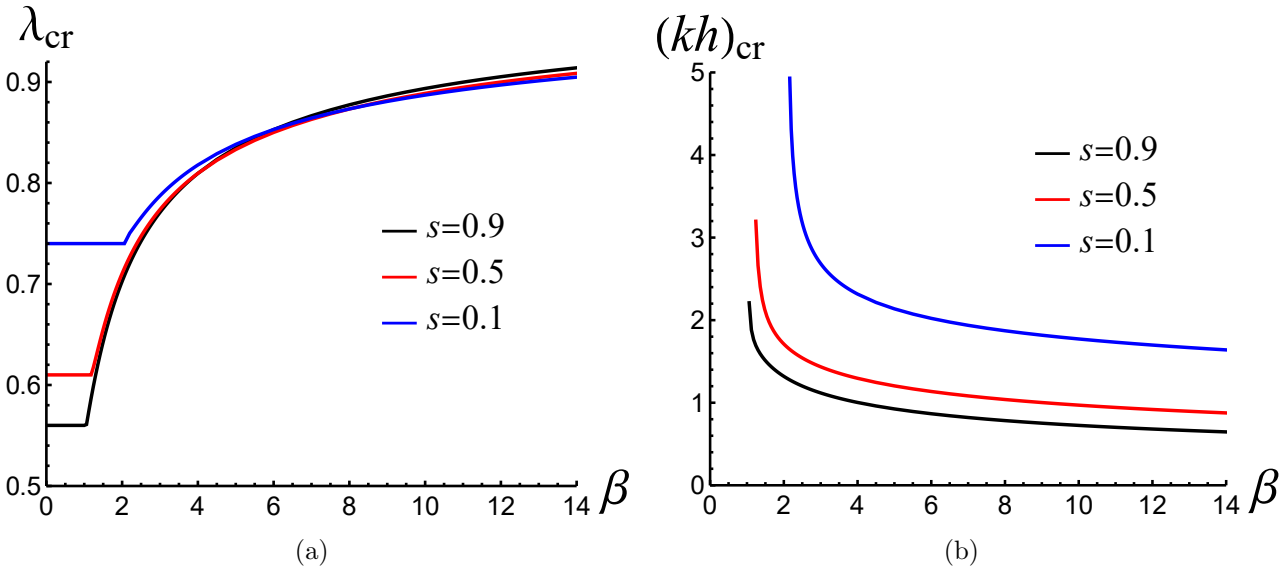

Figure 4: The critical stretch λ_{cr} and the critical wavenumber $(kh)_{cr}$ as functions of the modulus ratio β when $\theta_0 = 0$ and $s < 1$.

We see from Figure 4(b) that the critical wavenumber is a monotonically decreasing function of the modulus ratio β, regardless of the value of the anisotropy parameter s. This feature is also consistent with the results in the Goriely and Mihai (2021). In particular, as β goes to one, the critical wavenumber $(kh)_{cr}$ tends to infinity.

3.1.2. The case of $s > 1$

Next, we consider $s > 1$. In this case, from (2.16), we know that a director reorientation can take place at $\lambda = s^{-1/4}$. Hence, director reorientation will occur first before surface wrinkling if the critical stretch obtained from (3.10) (with $i = 1$) is lower than $s^{-1/4}$. Since λ_{cr} is dependent on β, we need to identify the transition where a director reorientation is induced first instead of surface wrinkling. This can be achieved by substituting $\lambda = s^{-1/4}$ into (3.10) (with $i = 1$).

Figure 5 shows that the critical modulus ratio β_{cr} depends monotonically on the anisotropy parameter s. We recall that there is no director reorientation provided $\beta > \beta_{cr}$. In practice, it provides a guidance to avoid or to trigger a director reorientation before surface wrinkling in the sample preparation process. For $\beta < \beta_{cr}$, the director will first rotate $\pi/2$ at $\lambda = s^{-1/4}$, changing its alignment from $\mathbf{E}_1$ to $\mathbf{E}_2$. In this case, we can use $(3.10)_2$ to find λ_{cr} and $(kh)_{cr}$. Subsequently, we plot in Figure 6 the curves of the critical stretch λ_{cr} and the critical wavenumber $(kh)_{cr}$ against the modulus ratio β when $s > 1$. Due to the presence of director reorientation, all curves exhibit a discontinuity at β_{cr} and as a consequence a discontinuity in both λ_{cr} and $(kh)_{cr}$.

We see from Figure 6(a) that director reorientation significantly delays wrinkling initiation. Moreover, as s increases, the magnitude of this delay effect also increases. When $\beta > \beta_{cr}$, the critical stretch is almost identical for different values of s. Notwithstanding, a careful observation reveals that λ_{cr} is an increasing function of s. If $\beta < \beta_{cr}$, the critical stretch decreases towards λ_{Biot}. Specifically, the black curve, corresponding to $s = 2$, will reach λ_{Biot} after β crosses β_{cr}. Figure 6(b) shows that the director reorientation prominently amplifies the critical wavenumber $(kh)_{cr}$. Also, the critical wavenumber $(kh)_{cr}$ decreases in s until the termination of each curve. Referring to Figure 2(a), it is expected that $(kh)_{cr} = 0$ when β is approaching unity. This explains why these curves terminate as β is getting small. Especially, for the black curve in Figure 6(b),

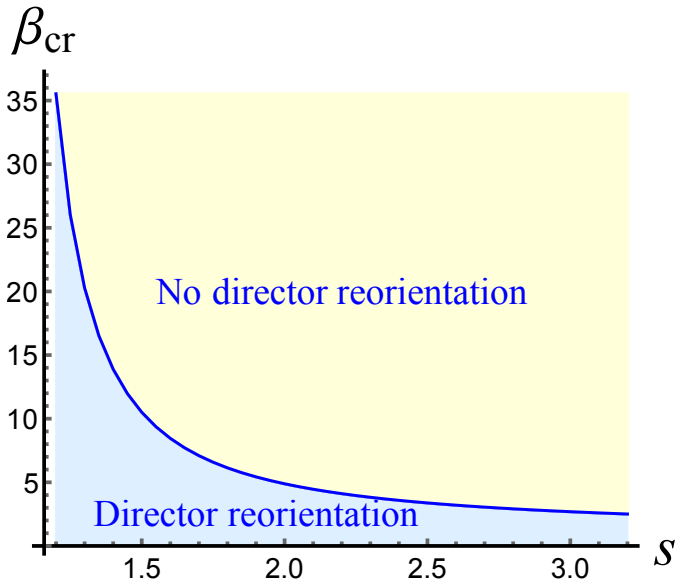

Figure 5: Dependence of the critical modulus ratio β_{cr} on the anisotropy parameter s if $\theta_0 = 0$ and $s > 1$.

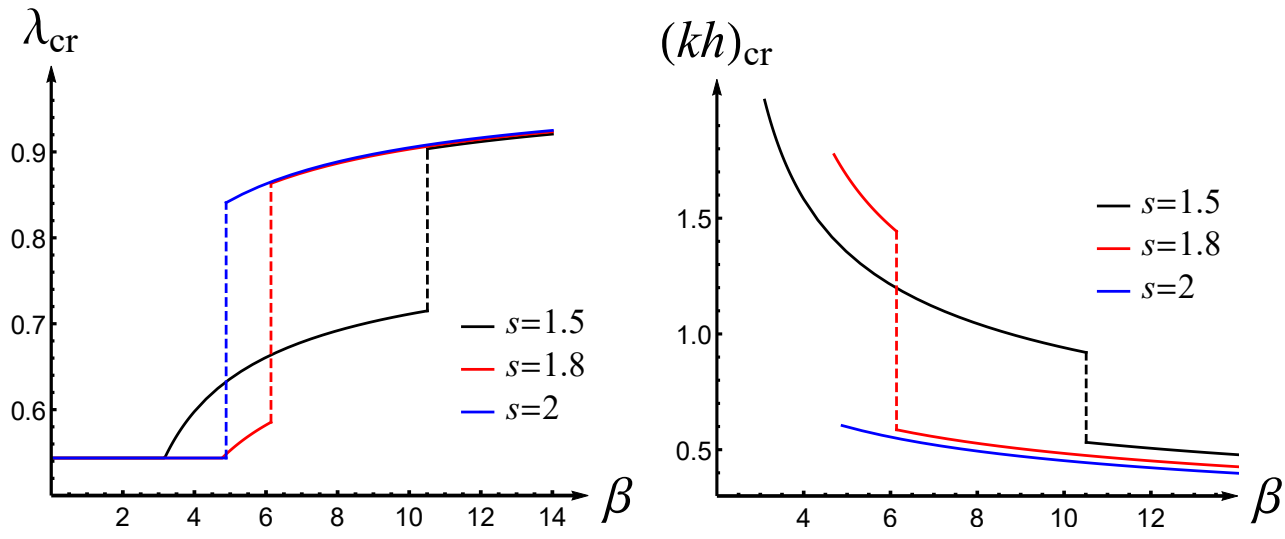

Figure 6: The critical stretch λ_{cr} and the critical wavenumber $(kh)_{cr}$ as functions of the modulus ratio β when $\theta_0 = 0$ and $s > 1$.

$(kh)_{cr}$ will jump from a finite value to 0 immediately after β passes β_{cr}.

3.2. Critical wrinkled state if the initial director is aligned in the vertical direction

Next, we study the bifurcations for $\theta_0 = \pi/2$. From (2.17), we see that that the director may rotate from $\mathbf{E}_2$ to $\mathbf{E}_1$ at $\lambda = s^{1/4}$ if $s < 1$. Similarly, we will distinguish the cases $s < 1$ and $s > 1$. As before, the pair $\{\lambda_{cr}, (kh)_{cr}\}$ can be identified by

$$f_i(\lambda, kh, \beta, s) = 0, \quad \frac{\partial f_i(\lambda, kh, \beta, s)}{\partial (kh)} = 0, \quad i = 3, 4. \tag{3.11}$$

3.2.1. The case of $s < 1$

In the case $s < 1$, we refer to the previous subsection and first determine the critical transition value $\beta_{\rm cr}$ where surface wrinkling will take place following a director reorientation. To this end, we directly substitute $\lambda = s^{1/4}$ into equations (3.11) (with $i = 3$). The result is shown in Figure 7, indicating that $\beta_{\rm cr}$ is a decreasing function of s. In particular, as $s \approx 1/2$, we find that $\beta_{\rm cr}$ is approaching zero, indicating that a further lower s fails to generate any director reorientation before surface wrinkling.

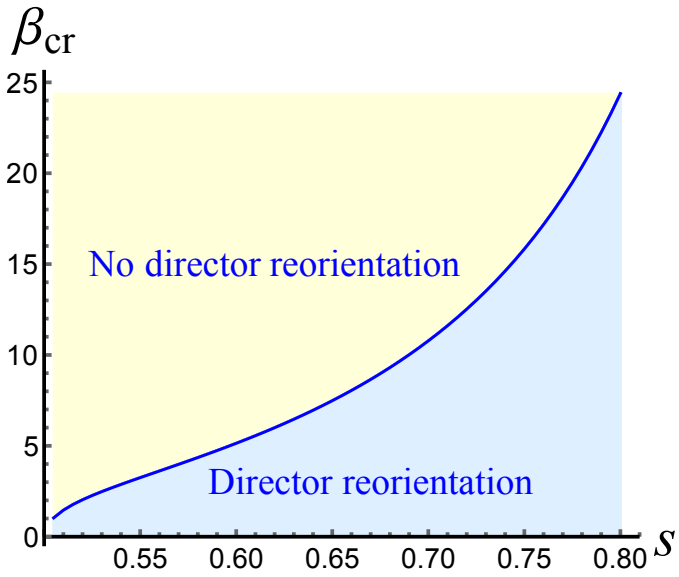

Figure 7: Dependence of the critical modulus ratio $\beta_{\rm cr}$ on the anisotropy parameter s if $\theta_0 = \pi/2$ and $s < 1$.

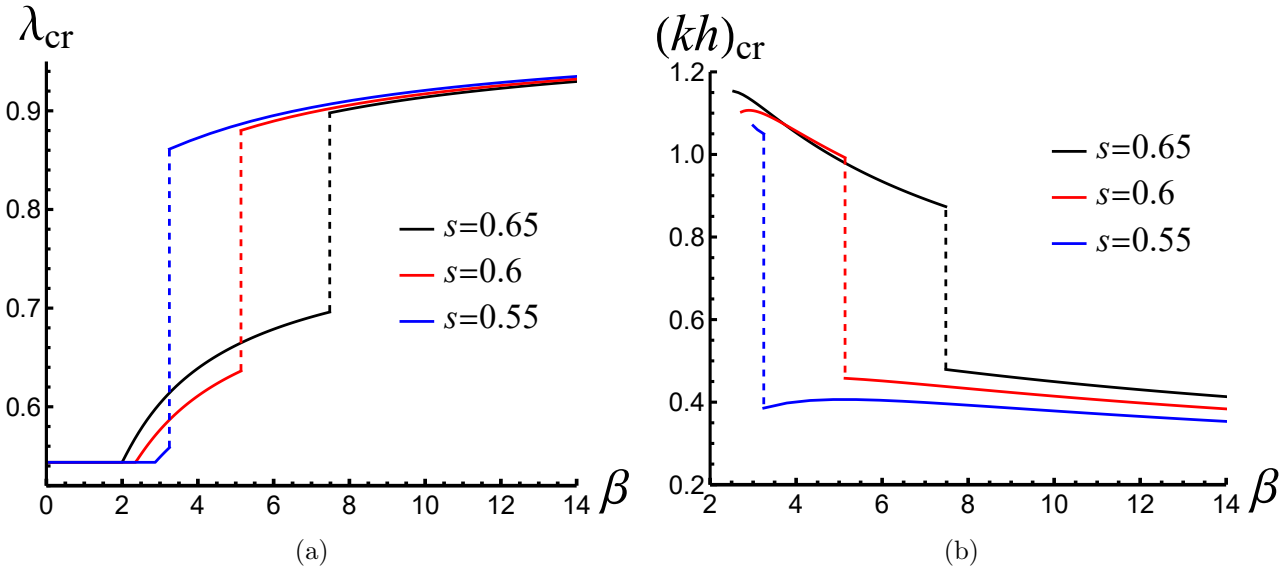

Figure 8: The critical stretch $\lambda_{\rm cr}$ and the critical wavenumber $(kh)_{\rm cr}$ as functions of the modulus ratio β when $\theta_0 = \pi/2$ and $s < 1$.

We show the curves of $\lambda_{\rm cr}$ and $(kh)_{\rm cr}$ in Figure 8 for varing β. Figure 8(a) illustrates that $\lambda_{\rm cr}$ slowly decreases with decreasing β until it passes the transition value $\beta_{\rm cr}$ where an obvious drop

in $\lambda_{\rm cr}$ is observed. This again implies that director reorientation indeed retards surface wrinkling. After that point, the $\lambda_{\rm cr}$-curve descends fast to $\lambda_{\rm Biot}$ as β further reduces. Figure 8(b) shows that the critical wavenumber $(kh)_{\rm cr}$ depends marginally on the modulus ration if $\beta > \beta_{\rm cr}$. Once more, the $(kh)_{\rm cr}$ curve stops at a special value of $\beta < \beta_{\rm cr}$ and therefore we have $(kh)_{\rm cr} = 0$ since then. When director reorientation happens, all curves display a remarkable upper jump, leading to a great increase in the value of $(kh)_{\rm cr}$. Combining the facts shown in Figures 6 and 8, we conclude that a director reorientation actually significantly delays surface wrinkling while producing more wrinkles.

3.2.2. The case of $s > 1$

Next, we consider the case $s > 1$ which excludes the possibility of director reorientation. In this case, we can directly obtain the exact solutions for $\lambda_{\rm cr}$ and $(kh)_{\rm cr}$ based on (3.11) with $i = 4$ and the results are displayed in Figure 9. We find that $\lambda_{\rm cr}$ monotonically decreases to the Biot value 0.5437 (the horizontal line) as β decreases. However, the critical wavenumber $(kh)_{\rm cr}$ increases monotonically with reducing β.

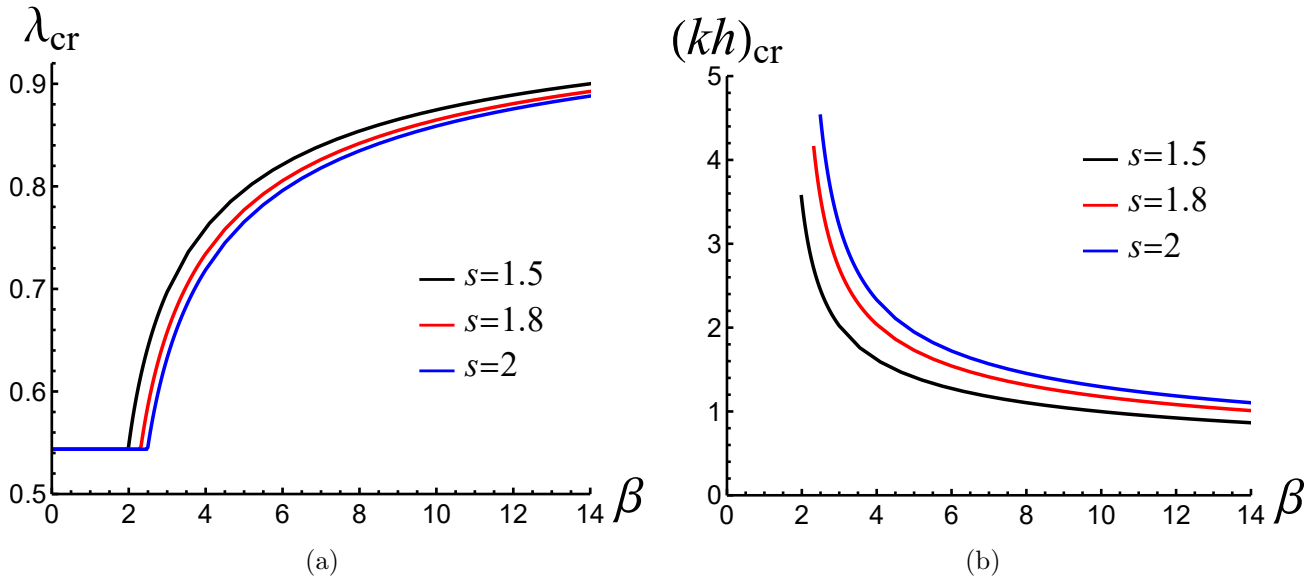

(a) (b)

Figure 9: The critical stretch $\lambda_{\rm cr}$ and the critical wavenumber $(kh)_{\rm cr}$ as functions of the modulus ratio β when $\theta_0 = \pi/2$ and $s > 1$.

3.3. The effect of the anisotropy parameter s

From Figures 4, 6, 8 and 9, we find that the LCE film makes a great difference in affecting the critical state, especially when there is a director reorientation. As the anisotropy parameter s is critical for distinguishing LCEs and isotropic materials, we investigate the influence of s on $\lambda_{\rm cr}$ and $(kh)_{\rm cr}$ and present the results in Figure 10. The discontinuities in all curves are caused by director reorientation. From the black curve corresponding to $\theta_0 = 0$, we conclude that an LCE film always creates a more stable bilayer compared to its isotropic counterpart if $s < 1$. When $1 < s < 1.3768$ (here the value 1.3768 can be found based on Figure 5 by taking $\beta = 15$), a sudden drop in $\lambda_{\rm cr}$ is observed and $\lambda_{\rm cr}$ reduces dramatically for increasing s. When $s > 1.3768$, $\lambda_{\rm cr}$ is always higher than the critical stretch with $s = 1$ and a greater s will make the bilayer unstable earlier. Meanwhile, the critical wavenumber $(kh)_{\rm cr}$ experiences a non-monotonic behaviour due

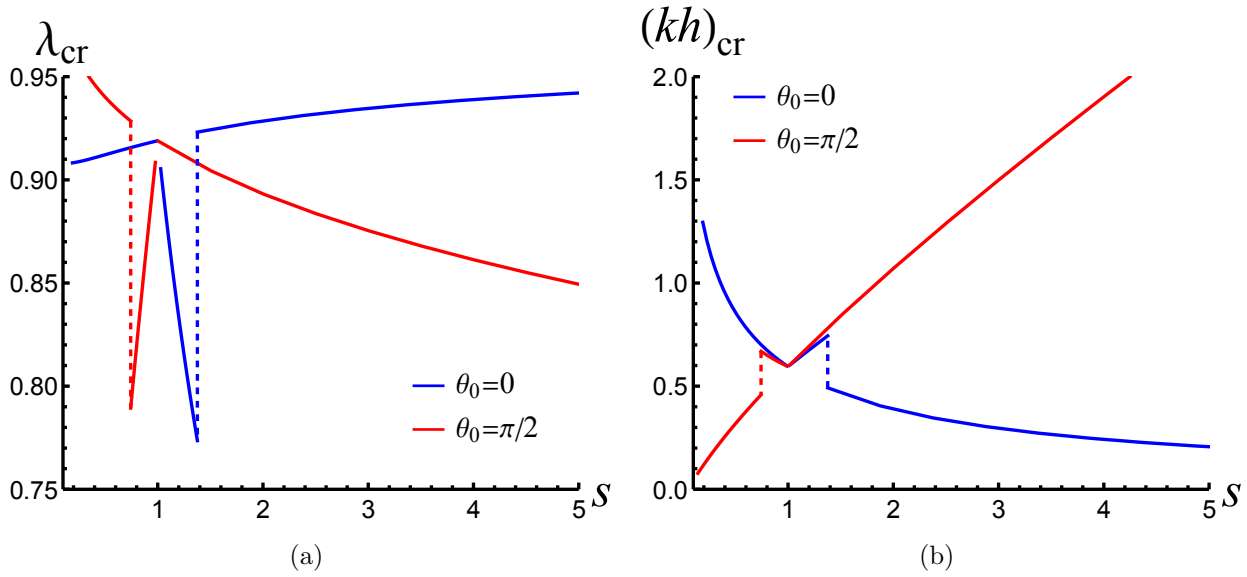

Figure 10: The critical stretch $\lambda_{\rm cr}$ and the critical wavenumber $(kh)_{\rm cr}$ as functions of the anisotropy parameter s for when $\beta = 15$ is fixed.

to director reorientation as s increases. When the initial director is aligned in the $\mathbf{E}_2$-direction ($\theta_0 = \pi/2$), the red curves impliy that for $0 < s < 0.7433$ (the value 0.7433 is identified based on Figure 7 by taking $\beta = 15$) we have an unstable bilayer compared to its isotropic counterpart ($s = 1$). For $0.7433 < s < 1$, a director reorientation takes place and it retards the onset of surface wrinkling. When $s > 1$, the $\lambda_{\rm cr}$-curve is monotonically decreasing in s, indicating that the bilayer is more stable.

In summary: A director reorientation will drastically delays surface wrinkling only if the anisotropy parameter s falls into a specific region, for example $(0.7433, 1) \cup (1, 1.3768)$ in Figure 10. Furthermore, if director reorientation is not granted, when $s < 0.7433$, the bilayer with $\theta_0 = 0$ is always more stable than its counterpart with $\theta_0 = \pi/2$. However, if $s > 1.3768$ the bilayer with $\theta_0 = \pi/2$ is more stable. Recalling that prolate liquid crystal molecules imply $s > 1$ while oblate molecules give $s < 1$, we conclude that when the major-axis of molecules coincides with the alignment of the director, a stable bilayer can be designed, and the associated wrinkled pattern is more wrinkled.

4. Asymptotic analysis

The exact bifurcation conditions (3.5) and (3.8) derived from the previous section are valid for all values of the geometric and material parameters. In practical applications, we are often in a regime with a thick soft substrate coated by a stiff thin film (Cai and Fu, 1999; Li et al., 2012; Goriely, 2017; Holland et al., 2018). Hence, it is of importance to study the case $\beta \gg 1$ in detail. In this regime an asymptotic analysis can also be performed. To this end, we further assume that $kh \to 0$ and $1/\beta \sim \mathcal{O}\left((kh)^3\right)$ (Cai and Fu, 1999; Liu and Dai, 2014; Alawiye et al., 2019; Goriely and Mihai, 2021).

From the analysis in Section 3 it is expected that, in the large β limit, surface wrinkling will take place when λ is close to 1 . Further, it has also been shown in Sections 3.1 and 3.2 that a director reorientation will retard the onset of surface wrinkling and create more wrinkles. We emphasize that both effects violate the assumption of small kh. Thus, we restrict our analysis to the case where no director reorientation is allowed. Replacing β by $\omega/(kh)^3$ with ω a constant of

$\mathcal{O}(1)$, we look for a solution to (3.5) and (3.8) depending only on the even orders of kh as follows (Goriely, et al. 2008; De Pascalis et al., 2011; Liu, 2023)

$$\lambda = 1 + \zeta_1(kh)^2 + \zeta_2(kh)^4 + \mathcal{O}\left((kh)^6\right), \tag{4.1}$$

where ζ_i $(i = 1, 2)$ are constants related to s and ω to be determined. In the following, we will again study separately the two cases $\theta_0 = 0$ and $\theta_0 = \pi/2$.

4.1. The initial director is aligned in the horizontal direction

We first look for solutions when $\theta_0 = 0$. To avoid director reorientation, we impose $s < 1$. In addition, it can be concluded from Figure 10(b) that kh is finite for small values of s. Therefore, we only consider $s < 1$ and $s \sim \mathcal{O}(1)$. Using (4.1) and replacing β by $\omega/(kh)^3$, the bifurcation condition (3.5) depends on the small parameter kh. We expand (3.5) at each order in kh to find:

$$\begin{aligned} \zeta_1 &= -\frac{6 + s^2\omega}{12s\omega}, \\ \zeta_2 &= \frac{31s^5\omega^2 + 4s^4\omega(2\omega - 45) + 180s^3\omega - 900s + 1440}{1440s^3\omega^2}. \end{aligned} \tag{4.2}$$

Substituting $\omega = \beta(kh)^3$ back into (4.2) gives rise to an expression for λ that solves the bifurcation condition (3.5):

$$\lambda = 1 - \frac{1}{2(kh)s\beta} - \frac{(kh)^2 s}{12} + \frac{(kh)^4 s(31s + 8)}{1440} - \frac{(5s - 8)}{8(kh)^2 s^3\beta^2} - \frac{1}{8\beta}(kh)(s - 1) + \mathcal{O}\left((kh)^6\right). \tag{4.3}$$

With the aid of $(3.10)_2$ with $i = 1$ we obtain the asymptotic solutions for $\lambda_{\rm cr}$ and $(kh)_{\rm cr}$:

$$\lambda_{\rm cr} = 1 - \frac{3^{2/3}}{4s^{1/3}\beta^{2/3}} - \frac{3^{1/3}(4s + 7)(5s - 8)}{160s^{5/3}\beta^{4/3}} - \frac{3^{2/3}}{8s^{1/3}\beta^{5/3}} + \mathcal{O}\left(\beta^{-2}\right), \tag{4.4}$$

$$(kh)_{\rm cr} = \frac{3^{1/3}}{s^{2/3}\beta^{1/3}} - \frac{(24 - 32s + 5s^2)}{20s^2\beta} + \mathcal{O}\left(\beta^{-5/3}\right). \tag{4.5}$$

It can be seen from (4.4) and (4.5) that, in addition to β, the anisotropy parameter s also appears at the leading-order, which explains both the delay to the bifurcation and the increase in wrinkles when $s < 1$.

As a check for this analysis, we set $s = 1$ in (4.4) and (4.5) to recover the solutions for surface wrinkling of a neo-Hookean film bonded to a neo-Hookean substrate up to the truncated order (Cai and Fu, 1999; Alawiye et al., 2019; Wang et al., 2023).

In Figure 11, a comparison between the exact solution and the asymptotic solution is given by specifying $s = 0.8$. A good agreement is found for both the critical stretch $\lambda_{\rm cr}$ and the critical wavenumber $(kh)_{\rm cr}$, especially when β is large enough.

4.2. The initial director is aligned in the vertical direction

Next, we consider the case $\theta_0 = \pi/2$. With a similar manner as before, we only consider $s > 1$ and $s \sim \mathcal{O}(1)$. Applying the same solution procedure, we find ζ_1 and ζ_2 in (4.1):

$$\begin{aligned} \zeta_1 &= -\frac{6s^2 + \omega}{12\omega s} \\ \zeta_2 &= \frac{180s^3\omega - 180s^2\omega - 900s^5 + 1440s^4 + 31s\omega^2 + 8\omega^2}{1440s^3\omega^2}. \end{aligned} \tag{4.6}$$

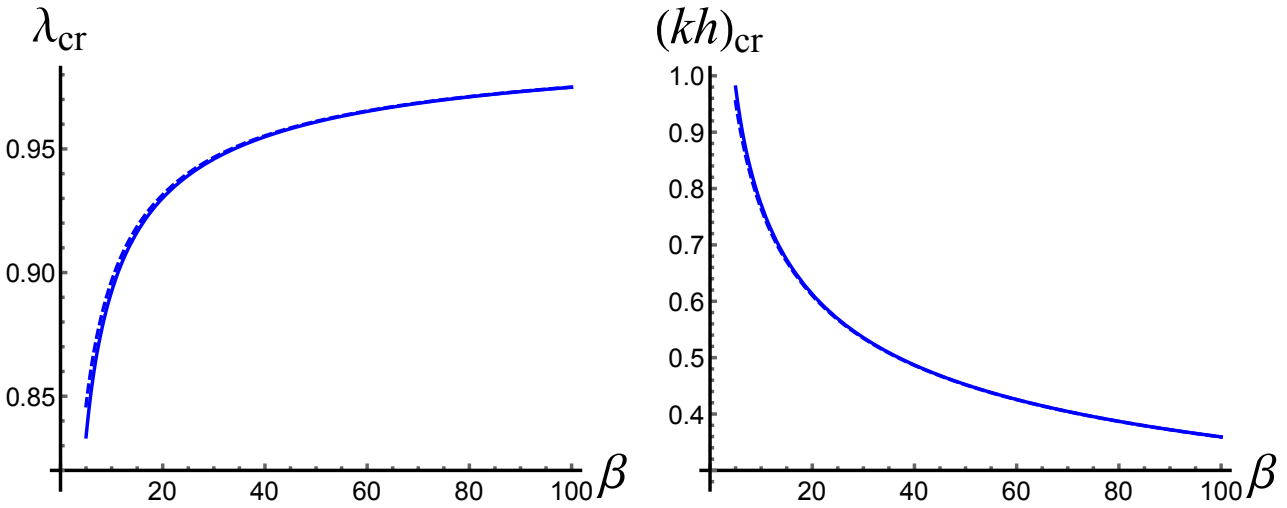

(a) (b)

Figure 11: Comparisons between the asymptotic solution (dashed line) and the exact solution (solid line) when $\theta_0 = 0$ and $s = 0.8$ where no director reorientation is allowed.

Inserting $\omega = \beta(kh)^3$ back into (4.6), the asymptotic solution satisfying the bifurcation condition (3.8) is found:

$$\lambda = 1 - \frac{s}{2(kh)\beta} - \frac{(kh)^2}{12s} + \frac{(kh)^4(31s+8)}{1440s^3} + \frac{s(8-5s)}{8(kh)^2\beta^2} + \frac{(s-1)(kh)}{8s\beta} + \mathcal{O}((kh)^6). \tag{4.7}$$

Based on $(3.11)_2$ with $i = 3$, we obtain the asymptotic solutions:

$$\lambda_{\rm cr} = 1 - \frac{3^{2/3}s^{1/3}}{4\beta^{2/3}} - \frac{3^{4/3}(s-12)}{160s^{1/3}\beta^{4/3}} - \frac{3^{2/3}s^{1/3}}{8\beta^{5/3}} + \mathcal{O}\left(\beta^{-2}\right), \tag{4.8}$$

$$(kh)_{\rm cr} = \frac{3^{1/3}s^{2/3}}{\beta^{1/3}} + \frac{(32s-29)}{20\beta} + \mathcal{O}\left(\beta^{-5/3}\right). \tag{4.9}$$

It can be seen that both the anisotropy parameter s and the modulus ratio β appear at the leading-order terms. Unlike (4.4) and (4.5), the anisotropy parameter s is now in the numerator, but since $s > 1$, the effect on the bifurcation and the number of wrinkles is the same as the previous case.

For $s = 1$, (4.8) and (4.9) reduce to the solutions for neo-Hookean bilayers (Cai and Fu, 1999; Alawiye et al., 2019; Wang et al., 2023). We illustrate a comparison between the exact solution and the asymptotic one in Figure 12. Good agreement between them, especially for large β, is a further validation for our asymptotic solutions.

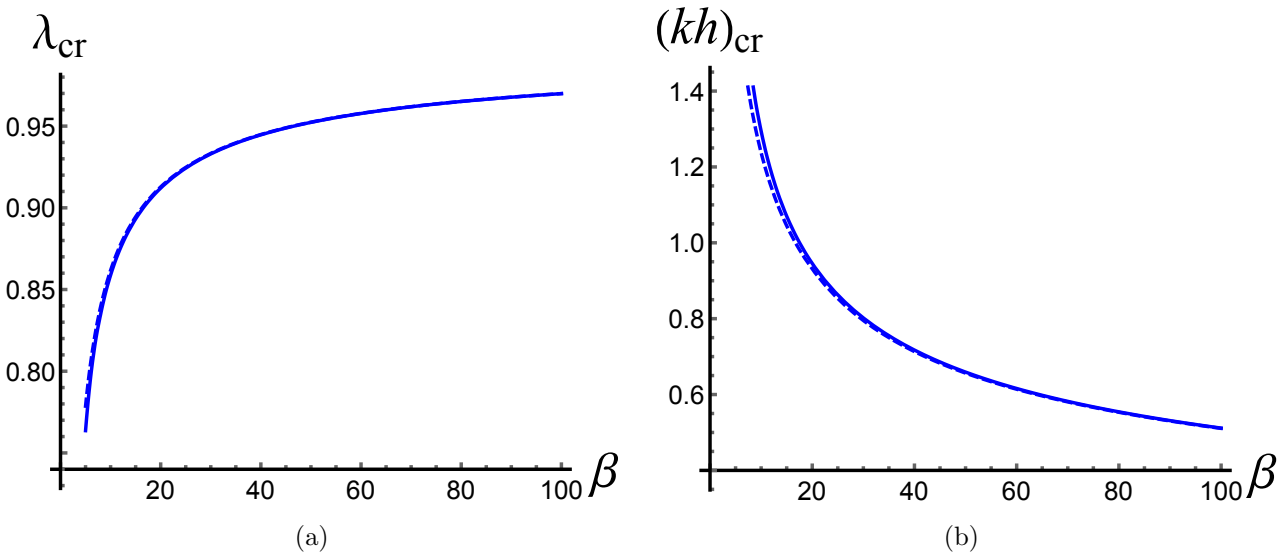

(a) (b)

Figure 12: Comparisons between the asymptotic solution (dashed line) and the exact solution (solid line) when $\theta_0 = \pi/2$ and $s = 2$ where no director reorientation is allowed.

5. Conclusion

The compression-induced surface wrinkling of a neo-Hookean substrate coated by an LCE film was studied within the framework of finite elasticity. By adopting a neo-classical model of LCEs proposed by Warner et al. (1988), we characterized the homogeneous solutions generated by axial compression before surface wrinkling. In particular, we assumed that the initial director is aligned in either the horizontal or the vertical direction. In this case, the deformed director is along either the horizontal or vertical direction (Mihai and Goriely, 2021). To carry out a bifurcation analysis, we considered both an increment in the displacement and an increment in the director, which required augmenting the classical incremental equations for the displacement with the incremental equations for the directors. An exact bifurcation condition for surface wrinkling was then obtained from which the critical stretch λ_{cr} as well as the critical wavenumber $(kh)_{cr}$ were identified.

Our analysis revealed the effect of two key parameters, namely, the modulus ratio between the LCE film and the substrate β and the anisotropy parameter s, on the critical wrinkled state. For the modulus ratio β, it is well known that a larger β promotes surface wrinkling but reduces the number of wrinkles. However, with directors, the situation changes. If $\theta_0 = 0$, the director is initially in the $\mathbf{E}_1$-direction, the critical stretch λ_{cr} increases as s increases without director reorientation. Moreover, the critical wavenumber $(kh)_{cr}$ is a decreasing function of s. If $\theta_0 = \pi/2$, a reserve trend is observed for both λ_{cr} and $(kh)_{cr}$.

We point out that there are two effective ways to increase the stability of LCE film-substrate bilayer. The first is to trigger director reorientation if s falls into some targeted regions. In this way, the onset of surface wrinkling will be delayed and the associated wavenumber will be amplified, with more wrinkles created. Moreover, if s is out of the targeted region, i.e. director reorientation is not admitted, we shall let the major-axis of liquid crystal molecules coincide with the alignment of the director. Correspondingly, we select $s > 1$ and $\theta_0 = \pi/2$ or $s < 1$ and $\theta_0 = 0$, then the bilayer is stabilised. Finally, we obtain some asymptotic solutions for λ_{cr} and $(kh)_{cr}$ as $kh \to 0$ and $1/\beta \sim \mathcal{O}\left((kh)^3\right)$, from which a clear picture on the combined effect of s and β emerges. Our work shows the importance of including the director in this type of instability and paves the way to a general incremental theory for LCEs.

It is further mentioned that surface wrinkling of LCE film-substrate bilayers can be complex due to a spacial distribution of the material parameter, a non-uniform distribution of initial directors, and three-dimensional geometry, etc. In spite of this, the current work aims to start from a simple setup and to further gain some fundamental knowledge of LCE wrinkling. For the issues of material inhomogeneity or stochastic properties, we refer to some recent papers Mihai and Goriely (2020); Liu et al. (2024), and leave these for future studies.

Acknowledgment

This work was supported by grants from the National Natural Science Foundation of China (Project Nos 12372072 and 12021002). Y.L. and A.G. acknowledge the UKRI Horizon Europe Guarantee MSCA (Marie Skłodowska-Curie Actions) Postdoctoral Fellowship (EPSRC Grant No. EP/Y030559/1). Q.J. acknowledges the Tianjin Research Innovation Project for Postgraduate Students (Grant No. 2022SKY072). For the purpose of Open Access, the author has applied a CC BY public copyright license to any Author Accepted Manuscript (AAM) version arising from this submission. We thank Prof. Angela Mihai at Cardiff University for valuable discussions and comments on this work.

Appendix A. The expressions of the coefficient matrices

The nonzero components of $\mathbf{M}_1$ are given by

$$
\begin{aligned}
&M_1^{11} = \mathrm{e}^{-\gamma_1 kh}\left(\gamma_1^2+\lambda^4(s-1)+1\right), \quad M_1^{12} = \mathrm{e}^{\gamma_1 kh}\left(\gamma_1^2+\lambda^4(s-1)+1\right),\\
&M_1^{13} = \mathrm{e}^{-\gamma_2 kh}\left(\gamma_2^2+\lambda^4(s-1)+1\right), \quad M_1^{14} = \mathrm{e}^{\gamma_2 kh}\left(\gamma_2^2+\lambda^4(s-1)+1\right),\\
&M_1^{21} = \gamma_1\mathrm{e}^{-\gamma_1 kh}\left(\gamma_1^2+\lambda^4(s-2)-2\right), \quad M_1^{22} = -\gamma_1\mathrm{e}^{\gamma_1 kh}\left(\gamma_1^2+\lambda^4(s-2)-2\right),\\
&M_1^{23} = \gamma_2\mathrm{e}^{-\gamma_2 kh}\left(\gamma_2^2+\lambda^4(s-2)-2\right), \quad M_1^{24} = -\gamma_2\mathrm{e}^{\gamma_2 kh}\left(\gamma_2^2+\lambda^4(s-2)-2\right),\\
&M_1^{31} = -\gamma_1, \quad M_1^{32} = \gamma_1, \quad M_1^{33} = -\gamma_2, \quad M_1^{34} = \gamma_2, \quad M_1^{35} = -1, \quad M_1^{36} = -\lambda^2,\\
&M_1^{41} = 1, \quad M_1^{42} = 1, \quad M_1^{43} = 1, \quad M_1^{44} = 1, \quad M_1^{45} = -1, \quad M_1^{46} = -1,\\
&M_1^{51} = \beta\left(\gamma_1^2+\lambda^4(s-1)+1\right), \quad M_1^{52} = \beta\left(\gamma_1^2+\lambda^4(s-1)+1\right),\\
&M_1^{53} = \beta\left(\gamma_2^2+\lambda^4(s-1)+1\right), \quad M_1^{54} = \beta\left(\gamma_2^2+\lambda^4(s-1)+1\right),\\
&M_1^{55} = -2, \quad M_1^{56} = -\lambda^4-1,\\
&M_1^{61} = \beta\gamma_1\left(\gamma_1^2+\lambda^4(s-2)-2\right), \quad M_1^{62} = -\beta\gamma_1\left(\gamma_1^2+\lambda^4(s-2)-2\right),\\
&M_1^{63} = \beta\gamma_2\left(\gamma_2^2+\lambda^4(s-2)-2\right), \quad M_1^{64} = -\beta\gamma_2\left(\gamma_2^2+\lambda^4(s-2)-2\right),\\
&M_1^{65} = -\lambda^4-1, M_1^{66} = -2\lambda^2.
\end{aligned}
\tag{A.1}
$$

The nonzero components of $\mathbf{M}_2$ are given by

$$
\begin{aligned}
&M_2^{11} = \frac{\mathrm{e}^{-\gamma_3 kh}\left(\gamma_3^2\left(\lambda^4 s^2+s-1\right)+\lambda^4 s^2\right)}{s^2}, \quad M_2^{12} = \frac{\mathrm{e}^{\gamma_3 kh}\left(\gamma_3^2\left(\lambda^4 s^2+s-1\right)+\lambda^4 s^2\right)}{s^2},\\
&M_2^{13} = \frac{\mathrm{e}^{-\gamma_4 kh}\left(\gamma_4^2\left(\lambda^4 s^2+s-1\right)+\lambda^4 s^2\right)}{s^2}, \quad M_2^{14} = \frac{\mathrm{e}^{\gamma_4 kh}\left(\gamma_4^2\left(\lambda^4 s^2+s-1\right)+\lambda^4 s^2\right)}{s^2},\\
&M_2^{21} = \frac{\gamma_3 \mathrm{e}^{-\gamma_3 kh}\left(\gamma_3^2\left(\lambda^4 s^2+s-1\right)+\lambda^4 s\left(-\lambda^4 s^2+s-3\right)\right)}{s^2},\\
&M_2^{22} = -\frac{\gamma_3 \mathrm{e}^{\gamma_3 kh}\left(\gamma_3^2\left(\lambda^4 s^2+s-1\right)+\lambda^4 s\left(-\lambda^4 s^2+s-3\right)\right)}{s^2},\\
&M_2^{23} = \frac{\gamma_4 \mathrm{e}^{-\gamma_4 kh}\left(\gamma_4^2\left(\lambda^4 s^2+s-1\right)+\lambda^4 s\left(-\lambda^4 s^2+s-3\right)\right)}{s^2},\\
&M_2^{24} = -\frac{\gamma_4 \mathrm{e}^{\gamma_4 kh}\left(\gamma_4^2\left(\lambda^4 s^2+s-1\right)+\lambda^4 s\left(-\lambda^4 s^2+s-3\right)\right)}{s^2},\\
&M_2^{31} = -\gamma_3, \quad M_2^{32} = \gamma_3, \quad M_2^{33} = -\gamma_4, \quad M_2^{34} = \gamma_4, \quad M_2^{35} = -1, \quad M_2^{36} = -\lambda^2,\\
&M_2^{41} = 1, \quad M_2^{42} = 1, \quad M_2^{43} = 1, \quad M_2^{44} = 1, \quad M_2^{45} = -1, \quad M_2^{46} = -1,\\
&M_2^{51} = \beta\left(\lambda^4 + \frac{\gamma_3^2\left(\lambda^4 s^2+s-1\right)}{s^2}\right), \quad M_2^{52} = \beta\left(\lambda^4 + \frac{\gamma_3^2\left(\lambda^4 s^2+s-1\right)}{s^2}\right),\\
&M_2^{53} = \beta\left(\lambda^4 + \frac{\gamma_4^2\left(\lambda^4 s^2+s-1\right)}{s^2}\right), \quad M_2^{54} = \beta\left(\lambda^4 + \frac{\gamma_4^2\left(\lambda^4 s^2+s-1\right)}{s^2}\right),\\
&M_2^{55} = -2\lambda^4, \quad M_2^{56} = -\lambda^4\left(\lambda^4+1\right),\\
&M_2^{61} = \frac{\beta\gamma_3\left(\gamma_3^2\left(\lambda^4 s^2+s-1\right)+\lambda^4 s\left(-\lambda^4 s^2+s-3\right)\right)}{s^2},\\
&M_2^{62} = \frac{\beta\gamma_3\left(\lambda^4 s\left(\lambda^4 s^2-s+3\right)-\gamma_3^2\left(\lambda^4 s^2+s-1\right)\right)}{s^2},\\
&M_2^{63} = \frac{\beta\gamma_4\left(\gamma_4^2\left(\lambda^4 s^2+s-1\right)+\lambda^4 s\left(-\lambda^4 s^2+s-3\right)\right)}{s^2},\\
&M_2^{64} = \frac{\beta\gamma_4\left(\lambda^4 s\left(\lambda^4 s^2-s+3\right)-\gamma_4^2\left(\lambda^4 s^2+s-1\right)\right)}{s^2},\\
&M_2^{65} = -\lambda^4\left(\lambda^4+1\right), \quad M_2^{66} = -2\lambda^6.
\end{aligned}
\tag{A.2}
$$

The nonzero components of $\mathbf{M}_3$ are given by

$$
\begin{aligned}
&M_3^{11} = s\mathrm{e}^{-\gamma_5 kh}\left(\lambda^4+\gamma_5^2\left(\lambda^4+s-1\right)\right), \quad M_3^{12} = s\mathrm{e}^{\gamma_5 kh}\left(\lambda^4+\gamma_5^2\left(\lambda^4+s-1\right)\right),\\
&M_3^{13} = s\mathrm{e}^{-\gamma_6 kh}\left(\lambda^4+\gamma_6^2\left(\lambda^4+s-1\right)\right), \quad M_3^{14} = s\mathrm{e}^{\gamma_6 kh}\left(\lambda^4+\gamma_6^2\left(\lambda^4+s-1\right)\right),\\
&M_3^{21} = \gamma_5\mathrm{e}^{-\gamma_5 kh}\left(\gamma_5^2 s\left(\lambda^4+s-1\right)+\lambda^4\left(-\lambda^4+s-3\right)\right),\\
&M_3^{22} = -\gamma_5\mathrm{e}^{\gamma_5 kh}\left(\gamma_5^2 s\left(\lambda^4+s-1\right)+\lambda^4\left(-\lambda^4+s-3\right)\right),\\
&M_3^{23} = \gamma_4\mathrm{e}^{-\gamma_4 kh}\left(\gamma_4^2 s\left(\lambda^4+s-1\right)+\lambda^4\left(-\lambda^4+s-3\right)\right),\\
&M_3^{24} = -\gamma_6\mathrm{e}^{\gamma_6 kh}\left(\gamma_6^2 s\left(\lambda^4+s-1\right)+\lambda^4\left(-\lambda^4+s-3\right)\right),\\
&M_3^{31} = -\gamma_5, \quad M_3^{32} = \gamma_5, \quad M_3^{33} = -\gamma_6, \quad M_3^{34} = \gamma_6, \quad M_3^{35} = -1, \quad M_3^{36} = -\lambda^2,\\
&M_3^{41} = 1, \quad M_3^{42} = 1, \quad M_3^{43} = 1, \quad M_3^{44} = 1, \quad M_3^{45} = -1, \quad M_3^{46} = -1,\\
&M_3^{51} = \beta s\left(\lambda^4+\gamma_5^2\left(\lambda^4+s-1\right)\right), \quad M_3^{52} = \beta s\left(\lambda^4+\gamma_5^2\left(\lambda^4+s-1\right)\right),\\
&M_3^{53} = \beta s\left(\lambda^4+\gamma_6^2\left(\lambda^4+s-1\right)\right), \quad M_3^{54} = \beta s\left(\lambda^4+\gamma_4^2\left(\lambda^4+s-1\right)\right),\\
&M_3^{55} = -2\lambda^4, \quad M_3^{56} = -\lambda^4\left(\lambda^4+1\right),\\
&M_3^{61} = \beta\gamma_5\left(\gamma_5^2 s\left(\lambda^4+s-1\right)+\lambda^4\left(-\lambda^4+s-3\right)\right),\\
&M_3^{62} = \beta\gamma_5\left(\lambda^4\left(\lambda^4-s+3\right)-\gamma_5^2 s\left(\lambda^4+s-1\right)\right),\\
&M_3^{63} = \beta\gamma_6\left(\gamma_6^2 s\left(\lambda^4+s-1\right)+\lambda^4\left(-\lambda^4+s-3\right)\right),\\
&M_3^{64} = \beta\gamma_6\left(\lambda^4\left(\lambda^4-s+3\right)-\gamma_6^2 s\left(\lambda^4+s-1\right)\right),\\
&M_3^{65} = -\lambda^4\left(\lambda^4+1\right), \quad M_3^{66} = -2\lambda^6,
\end{aligned}
\tag{A.3}
$$

where the eigenvalues γ_5 and γ_6 read

$$
\gamma_5 = \left(\frac{\lambda^4+3-2s-\sqrt{\left(\lambda^4+3\right)^2-8\left(\lambda^4+1\right)s}}{2s(\lambda^4+s-1)}\right)^{1/2}\lambda^2,
$$

$$
\gamma_6 = \left(\frac{\lambda^4+3-2s+\sqrt{\left(\lambda^4+3\right)^2-8\left(\lambda^4+1\right)s}}{2s(\lambda^4+s-1)}\right)^{1/2}\lambda^2.
$$

The nonzero components of $\mathbf{M}_4$ are given by

$$
\begin{aligned}
&M_4^{11} = \frac{\mathrm{e}^{-\gamma_7 kh}\left(-\lambda^4 + (\gamma_7^2+1)\,s^2 + \lambda^4 s\right)}{s}, \quad M_4^{12} = \frac{\mathrm{e}^{\gamma_7 kh}\left(-\lambda^4 + (\gamma_7^2+1)\,s^2 + \lambda^4 s\right)}{s},\\
&M_4^{13} = \frac{\mathrm{e}^{-\gamma_8 kh}\left(-\lambda^4 + (\gamma_8^2+1)\,s^2 + \lambda^4 s\right)}{s}, \quad M_4^{14} = \frac{\mathrm{e}^{\gamma_8 kh}\left(-\lambda^4 + (\gamma_8^2+1)\,s^2 + \lambda^4 s\right)}{s},\\
&M_4^{21} = \frac{\gamma_7\mathrm{e}^{-\gamma_7 kh}\left(-2\lambda^4 + (\gamma_7^2-2)\,s^2 + \lambda^4 s\right)}{s}, \quad M_4^{22} = -\frac{\gamma_7\mathrm{e}^{\gamma_7 kh}\left(-2\lambda^4 + (\gamma_7^2-2)\,s^2 + \lambda^4 s\right)}{s},\\
&M_4^{23} = \frac{\gamma_8\mathrm{e}^{-\gamma_8 kh}\left(-2\lambda^4 + (\gamma_8^2-2)\,s^2 + \lambda^4 s\right)}{s}, \quad M_4^{24} = -\frac{\gamma_8\mathrm{e}^{\gamma_8 kh}\left(-2\lambda^4 + (\gamma_8^2-2)\,s^2 + \lambda^4 s\right)}{s},\\
&M_4^{31} = -\gamma_7, \quad M_4^{32} = \gamma_7, \quad M_4^{33} = -\gamma_8, \quad M_4^{34} = \gamma_8, \quad M_4^{35} = -1, \quad M_4^{36} = -\lambda^2,\\
&M_4^{41} = 1, \quad M_4^{42} = 1, \quad M_4^{43} = 1, \quad M_4^{44} = 1, \quad M_4^{45} = -1, \quad M_4^{46} = -1,\\
&M_4^{51} = \beta\left(\lambda^4 + \gamma_7^2 s - \frac{\lambda^4}{s} + s\right), \quad M_4^{52} = \beta\left(\lambda^4 + \gamma_7^2 s - \frac{\lambda^4}{s} + s\right),\\
&M_4^{53} = \beta\left(\lambda^4 + \gamma_8^2 s - \frac{\lambda^4}{s} + s\right), \quad M_4^{54} = \beta\left(\lambda^4 + \gamma_8^2 s - \frac{\lambda^4}{s} + s\right),\\
&M_2^{55} = -2, \quad M_4^{56} = -\lambda^4 - 1,\\
&M_4^{61} = \frac{\beta\gamma_7\left(-2\lambda^4 + (\gamma_7^2-2)\,s^2 + \lambda^4 s\right)}{s}, \quad M_4^{62} = -\frac{\beta\gamma_7\left(-2\lambda^4 + (\gamma_7^2-2)\,s^2 + \lambda^4 s\right)}{s},\\
&M_4^{63} = \frac{\beta\gamma_8\left(-2\lambda^4 + (\gamma_8^2-2)\,s^2 + \lambda^4 s\right)}{s}, \quad M_4^{64} = -\frac{\beta\gamma_8\left(-2\lambda^4 + (\gamma_8^2-2)\,s^2 + \lambda^4 s\right)}{s},\\
&M_4^{65} = -\lambda^4 - 1, \quad M_4^{66} = -2\lambda^2,
\end{aligned}
\tag{A.4}
$$

where the eigenvalues γ_7 and γ_8 read

$$
\begin{aligned}
\gamma_7 &= \left(\frac{3\lambda^4 + s^2 - 2\lambda^4 s - \sqrt{s^4 + 2\lambda^4 s^2(3-4s) + \lambda^8(9-8s)}}{2s^2}\right)^{1/2},\\
\gamma_8 &= \left(\frac{3\lambda^4 + s^2 - 2\lambda^4 s + \sqrt{s^4 + 2\lambda^4 s^2(3-4s) + \lambda^8(9-8s)}}{2s^2}\right)^{1/2}.
\end{aligned}
$$

References

Agrawal, A., Luchette, P., Palffy-Muhoray, P., Biswal, S.L., Chapman, W.G., Verduzco, R. 2012. Surface wrinkling in liquid crystal elastomers. Soft Matter, 8(27), 7138–7142.

Agrawal, A., Yun, T., Pesek, S.L., Chapman, W.G., Verduzco, R. 2014. Shape-responsive liquid crystal elastomer bilayers. Soft Matter, 10(9), 1411–1415.

Alawiye, H., Kuhl, E., Goriely, A. 2019. Revisiting the wrinkling of elastic bilayers I: linear analysis. Philosophical Transactions of the Royal Society A: Mathematical, Physical and Engineering Sciences, 377, 20180076.

Anderson, D.R., Carlson, D.E., Fried, E. 1999. A continuum-mechanical theory for nematic elastomers. Journal of Elasticity, 56(1), 33–58.

Andres, S., Steinmann, P., Budday, S. 2018. The origin of compression influences geometric instabilities in bilayers. Proceedings of the Royal Society A: Mathematical, Physical and Engineering Sciences, 474(2217), 20180267.

Ball, J.M., Bedford, S.J. 2015. Discontinuous order parameters in liquid crystal theories. Molecular Crystals and Liquid Crystals, 612(1), 1–23.

Barnes, M., Feng, F., Biggins, J. 2023. Surface Instability in a Nematic Elastomer Physical Review Letters, 131, 238101.

Biot, M.A. 1963. Surface instability of rubber in compression. Applied Scientific Research, 12, 168–182.

Biot, M.A. 1965. Mechanics of Incremental Deformations, Jonh Wiley & Sons, New York.

Bladon, P., Terentjev, E.M., Warner, M. 1993. Transitions and instabilities in liquid crystal elastomers. Physical Review E, 47(6), R3838-R3840.

Budday, S., Kuhl, E., Hutchinson, J.W. 2015. Period-doubling and period-tripling in growing bilayered systems. Philosophical Magazine, 95, 3208–3224.

Cai, Z., Fu, Y.B. 1999. On the imperfection sensitivity of a coated elastic half-space. Proceedings of the Royal Society of London. Series A: Mathematical, Physical and Engineering Sciences, 455(1989), 3285–3309.

Cao, Y.P., Hutchinson, J.W. 2012. Wrinkling phenomena in neo-Hookean film/substrate bilayers. Journal of Applied Mechanics-Transactions of the Asme, 79(3), 031019.

Chen, M., Hou, Y., An, R., Qi, H.J., Zhou, K. 2023. 4D printing of reprogrammable liquid crystal elastomers with synergistic photochromism and photoactuation. Advanced Materials, in press, DOI: 10.1002/adma.202303969.

Chen, Y.C., Fried, E., 2006. Uniaxial nematic elastomers: constitutive framework and a simple application. Proc. R. Soc. A 462, 20140494.

Chen, Y., Kuenstler, A.S., Hayward, R.C., Jin, L. 2022. Formation of rolls from liquid crystal elastomer bistrips. Soft Matter, 18(21), 4077-4089.

Conti, S., DeSimone, A., Dolzmann, G. 2002. Soft elastic response of stretched sheets of nematic elastomers: a numerical study. Journal of the Mechanics and Physics of Solids, 50(7), 1431–1451.

De Pascalis, R., Destrade, M., Goriely, A. 2011. Nonlinear correction to the Euler buckling formula for compressed cylinders with guided-guided end conditions. Journal of Elasticity, 102, 191–200.

De Gennes, P.G., Hébert, M., Kant, R. 1997. Artificial muscles based on nematic gels. In Macromolecular Symposia, 113(1), 39-49.

DeSimone, A., Gidoni, P., Noselli, G. 2015. Liquid crystal elastomer strips as soft crawlers. Journal of the Mechanics and Physics of Solids, 84, 254–272.

Fried, E., Korchagin, V. 2002. Striping of nematic elastomer. International Journal of Solids and Structures, 39, 3451–3467.

Fried, E., Sellers, S. 2006. Soft elasticity is not necessary for striping in nematic elastomers. Journal of Applied Physics, 100(4), 043521.

Fu, Y.B., Jin, L., Goriely, A. 2021. Necking, beading, and bulging in soft elastic cylinders. Journal of the Mechanics and Physics of Solids, 147, 104250.

Fu, Y.X., Wang, Y.S., Fu, Y.B. 2023. New mountain ridge modes in a film/substrate bilayer. Mathematics and Mechanics of Solids, DOI: 10.1177/10812865231208414, 1–15.

Fu, Y.B., Ogden, R.W. 1999. Nonlinear stability analysis of pre-stressed elastic bodies. Continuum Mechanics and Thermodynamics, 11(3), 141–172.

Fu, C., Xu, F., Huo, Y. 2018. Photo-controlled patterned wrinkling of liquid crystalline polymer films on compliant substrates. International Journal of Solids and Structures, 132, 264–277.

Goriely, A., 2017. The Mathematics and Mechanics of Biological Growth. Springer, New York.

Goriely, A., Mihai, L.A. 2021. Liquid crystal elastomers wrinkling. Nonlinearity, 34(8), 5599–5629.

Goriely, A., Moulton, D.E., Mihai, L.A. 2023. A rod theory for liquid crystalline elastomers. Journal of Elasticity, 153, 509–532.

Goriely, A., Vandiver, R., Destrade, M. Nonlinear Euler buckling, 2008. Proceedings of the Royal Society A: Mathematical, Physical and Engineering Sciences, 464, 3003–3019.

Holland, M., Budday, S., Goriely, A., Kuhl, E., 2018. Symmetry breaking in wrinkling patterns: Gyri are universally thicker than sulci. Physical Review Letters, 121, 228002.

Jia, F., Pearce, S.P., Goriely, A., 2018. Curvature delays growth-induced wrinkling. Physical Review E, 98, 033003

Jin, L., Liu, Y., Cai, Z., 2019. Post-buckling analysis on growing tubular tissues: A semi-analytical approach and imperfection sensitivity. International Journal of Solids and Structures, 162, 121–134.

Krieger, M.S., Dias, M.A. 2019. Tunable wrinkling of thin nematic liquid crystal elastomer sheets. Physical Review E, 100(2), 022701.

Kundler, I., Finkelmann, H. 1995. Strain-induced director reorientation in nematic liquid single crystal elastomers. Macromolecular rapid communications, 16(9), 679–686.

Li, B., Cao, Y.P., Feng, X.Q., Gao H., 2012. Mechanics of morphological instabilities and surface wrinkling in soft materials: a review. Soft Matter 8, 5728.

Lee, V., Wihardja, A., Bhattacharya, K. 2023. A macroscopic constitutive relation for isotropic-genesis, polydomain liquid crystal elastomers. Journal of the Mechanics and Physics of Solids, 179, 105369.

Liu, S., Huang, K., Wang, K., Wang, B. 2022. Programmable deformation of liquid crystal elastomer plates subjected to concentrated light illumination. Mechanics of Materials, 175, 104501.

Liu, Y. 2023. Higher order solution to the Euler buckling threshold for compressible hyperelastic bilayers. Acta Mechanica Sinica, 39(8), 422379.

Liu, Y., Dai, H.-H. 2014. Compression of a hyperelastic layer-substrate structure: Transitions between buckling and surface modes. International Journal of Engineering Science, 80, 74–89.

Liu, Y., Dorfmann, L. 2023. Localized necking and bulging of finitely deformed residually stressed solid cylinder. Mathematics and Mechanics of Solids, DOI: 10.1177/10812865231186951, 1–23.

Liu, R.C., Liu, Y., Cai, Z. 2021. Influence of the growth gradient on surface wrinkling and pattern transition in growing tubular tissues. Proceedings of the Royal Society A: Mathematical, Physical and Engineering Sciences, 477, 20210441.

Liu, R.C., Liu, Y., Goriely, A. 2024. Surface wrinkling of a film coated to a graded substrate. Journal of the Mechanics and Physics of Solids, 186, 105603.

Liu, Y., Ma, W., Dai, H.-H. 2020. On a consistent finite-strain plate model of nematic liquid crystal elastomers. Journal of the Mechanics and Physics of Solids, 145, 104169.

Liu, Y., Ma, W., Dai, H.-H. 2021. Bending-induced director reorientation of a nematic liquid crystal elastomer bonded to a hyperelastic substrate. Journal of Applied Physics, 129(10), 104701.

Liu, H., Tian, H., Shao, J., Wang, Z., Li, X., Wang, C., Chen, X. 2020. An electrically actuated soft artificial muscle based on a high-performance flexible electrothermal film and liquid-crystal elastomer. ACS Applied Materials & Interfaces, 12(50), 56338–56349.

Mahardika, N., Raistrick, T., Mihai, L. A., Wang, H. 2024. All-atom molecular dynamics simulations of nematic liquid crystal elastomers. International Journal of Solids and Structures, 291, 112717.

Mbanga, B.L., Ye, F., Selinger, J.V., Selinger, R.L. 2010. Modeling elastic instabilities in nematic elastomers. Physical Review E, 82(5), 051701.

Mihai, L.A., Gablier, A., Terentjev, E., Goriely, A. (2023). Anti-Hertz bulging of actuated liquid crystal elastomers. Extreme Mechanics Letters, 64, 102066.

Mihai, L.A., Goriely, A. 2020. Likely striping in stochastic nematic elastomers. Mathematics and Mechanics of Solids, 25(10), 1851–1872.

Mihai, L.A., Goriely, A. 2020. A plate theory for nematic liquid crystalline solids. Journal of the Mechanics and Physics of Solids, 144, 104101.

Mihai, L.A., Goriely, A. 2021. Instabilities in liquid crystal elastomers. MRS Bulletin, 46, 784–794.

Mihai, L.A., Mistry, D., Raistrick, T., Gleeson, H. F., Goriely, A. 2022. A mathematical model for the auxetic response of liquid crystal elastomers. Philosophical Transactions of the Royal Society A: Mathematical, Physical and Engineering Sciences, 380, 20210326.

Mihai, L.A., Raistrick, T., Gleeson, H. F., Mistry, D., Goriely, A. 2023. A predictive theoretical model for stretch-induced instabilities in liquid crystal elastomers. Liquid Crystals, 50(7–10), 1426–1438.

Mitchell, G.R., Davis, F., Guo, W., 1993. Strain-induced transitions in liquid-crystal elastomers. Physical Review Letters, 71, 2947–2950.

Ogden, R.W. 1984, Non-Linear Elastic Deformations, New York: Ellis Horwood.

Pang, X., Lv, J. A., Zhu, C., Qin, L., Yu, Y. 2019. Photodeformable azobenzene-containing liquid crystal polymers and soft actuators. Advanced Materials, 31(52), 1904224.

Peng, Z., Jiang, Y., Chen, Y., Huo, Y. 2023. Attenuating liquid crystal elastomers' stress concentration by programming initial orientation. International Journal of Mechanical Sciences, 249, 108274.

Potekhin, A., Wang, C. 2021. Numerical simulation and experimental validation of bending and curling behaviors of liquid crystal elastomer beams under thermal actuation. Applied Physics Letters, 118, 241903.

Qing, X., Liu, Y., Wei, J., Zheng, R., Zhu, C., Yu, Y. 2019. Phototunable Morpho butterfly microstructures modified by liquid crystal polymers. Advanced Optical Materials, 7(3), 1801494.

Soni, H., Pelcovits, R.A., Powers, T.R. 2016. Wrinkling of a thin film on a nematic liquid-crystal elastomer. Physical Review E, 94(1), 012701.

Sonnet, A.M., Virga, E.G. 2022. Model for a Photoresponsive Nematic Elastomer Ribbon. Journal of Elasticity, 1–28.

Stewart, P.S., Waters, S.L., El Sayed, T., Vella, D., Goriely, A. (2016). Wrinkling, creasing, and folding in fiber-reinforced soft tissues. Extreme Mechanics Letters, 8, 22-29.

Tian, H., Wang, Z., Chen, Y., Shao, J., Gao, T., Cai, S. 2018. Polydopamine-coated main-chain liquid crystal elastomer as optically driven artificial muscle. ACS applied materials & interfaces, 10(9), 8307–8316.

Urayama, K., Kondo, H., Arai, Y.O., Takigawa, T. 2005. Electrically driven deformations of nematic gels. Physical Review E, 71(5), 051713.

Urayama, K., Honda, S., Takigawa, T. 2006. Deformation coupled to director rotation in swollen nematic elastomers under electric fields. Macromolecules, 39(5), 1943–1949.

Wang, G., Liu, Y., Fu, Y.B. 2023. A refined model for the buckling of film/substrate bilayers. Mathematics and Mechanics of Solids, 28(1), 313-330.

Wang, M., Han, Y., Guo, L.X., Lin, B.P., Yang, H. 2019. Photocontrol of helix handedness in curled liquid crystal elastomers. Liquid Crystals, 46(8), 1231–1240.

Wang, Y., An, J., Lee, H. 2022. Recent advances in molecular programming of liquid crystal elastomers with additive manufacturing for 4D printing. Molecular Systems Design & Engineering, 7(12), 1588–1601.

Wang, Y., Huang, X., Zhang, J., Bi, M., Zhang, J., Niu, H., Jiang, H. 2017. Two-step crosslinked liquid-crystalline elastomer with reversible two-way shape memory characteristics. Molecular Crystals and Liquid Crystals, 650(1), 13–22.

Wang, Z., Boechler, N., Cai, S. 2022. Anisotropic mechanical behavior of 3D printed liquid crystal elastomer. Additive Manufacturing, 52, 102678.

Wang, Z., Chehade, A.E.H., Govindjee, S., Nguyen, T.D. 2022. A nonlinear viscoelasticity theory for nematic liquid crystal elastomers. Journal of the Mechanics and Physics of Solids, 163, 104829.

Wang, Z., Tian, H., He, Q., Cai, S. 2017. Reprogrammable, reprocessible, and self-healable liquid crystal elastomer with exchangeable disulfide bonds. ACS applied materials & interfaces, 9(38), 33119–33128.

Wang, Z., He, Q., Wang, Y., Cai, S. 2019. Programmable actuation of liquid crystal elastomers via "living" exchange reaction. Soft Matter, 15(13), 2811–2816.

Ware, T.H., Biggins, J.S., Shick, A.F., Mark Warner, M., White, T.J. 2016. Localized soft elasticity in liquid crystal elastomers. Nature Communications, 7, 10781.

Warner, M., Gelling, K.P., Vilgis, T.A. 1988. Theory of nematic networks. The Journal of Chemical Physics, 88, 4008–4013.

Warner, M., Terentjev, E.M. 2007. Liquid crystal elastomers. Oxford University Press.

White, T.J., Broer, D.J. 2015. Programmable and adaptive mechanics with liquid crystal polymer networks and elastomers. Nature Materials, 14, 1087–1098.

Wu, J., Xiao, Y., Zhang, Y., Fang, D. 2023. A constitutive model of liquid crystal elastomers with loading-history dependence. Journal of the Mechanics and Physics of Solids, 174, 105258.

Xiao, Y., Wu, J., Zhang, Y. 2023. Recent advances in the design, fabrication, actuation mechanisms and applications of liquid crystal elastomers. Soft Science, 3, 11.

Xu, F., Zhao, S. 2020. Thermal wrinkling of liquid crystal polymer shell/core spheres. Extreme Mechanics Letters, 40, 100860.

Xu, Y., Zhang, Y., Huo, Y. 2020. Electric-field induced deformation and bending in nematic elastomer strips with orientation gradient. International Journal of Solids and Structures, 202, 243–259.

Yan, Z., Ji, X., Wu, W., Wei, J., Yu, Y. 2012. Light-switchable behavior of a microarray of azobenzene liquid crystal polymer induced by photodeformation. Macromolecular Rapid Communications, 33(16), 1362–1367.

Zeng, H., Wani, O. M., Wasylczyk, P., Priimagi, A. 2018. Light-driven, caterpillar-inspired miniature inching robot. Macromolecular Rapid communications, 39(1), 1700224.

Zhai, F., Feng, Y., Li, Z., Xie, Y., Ge, J., Wang., H., Qiu, W., Feng, W. 2021. 4D-printed untethered self-propelling soft robot with tactile perception: Rolling, racing, and exploring. Matter, 4(10), 3313–3326.

Zhang, Y., Xuan, C., Jiang, Y., Huo, Y. 2019. Continuum mechanical modeling of liquid crystal elastomers as dissipative ordered solids. Journal of the Mechanics and Physics of Solids, 126, 285–303.

Zhao, S., Xu, F, Fu, C., Huo, Y. 2019. Controllable wrinkling patterns on liquid crystal polymer film/substrate systems by laser illumination. Extreme Mechanics Letters, 30, 100502.

Zhao, S., Chen, Y., Huo, Y. 2023. Formation of lamellar domains in liquid crystal elastomers under compression. International Journal of Mechanical Sciences, 247, 108185.

Zhao, T., Wang, J., Fan, Y., Dou, W. 2022. Helical liquid crystal elastomer miniature robot with photocontrolled locomotion. Advanced Materials Technologies, 7(10), 2200222.